

## Article

# Mapping Cropland Abandonment in the Cloudy Hilly Regions Surrounding the Southwest Basin of China

Yali Wei \*, Junjie Wen, Qunchao Zhou, Yan Zhang and Gaocheng Dong

College of Resource, Sichuan Agricultural University, Chengdu 611130, China; wenjunjie@stu.sicau.edu.cn (J.W.); zhouqunchao@stu.sicau.edu.cn (Q.Z.); 2022306077@stu.sicau.edu.cn (Y.Z.); donggaocheng@stu.sicau.edu.cn (G.D.)

\* Correspondence: weiyali@sicau.edu.cn

**Abstract:** Cropland is a vital resource intricately connected to food security. Currently, the issue of cropland abandonment poses a serious threat to food production and supply, presenting a significant challenge to rural economies and the stability of the food supply chain. The hilly and cloudy regions of southwest China are particularly affected by cropland abandonment, presenting significant challenges in accurately mapping the distribution of abandoned cropland due to fragmentation and heavy cloud pollution. Therefore, this study focuses on Mingshan County, located in Ya'an City, Sichuan Province, China, as the study area. Utilizing Google Earth Engine (GEE) and a random forest algorithm, a method integrating multi-source data from Landsat 8, Sentinel-2, and Sentinel-1 is proposed to extract abandoned cropland spanning from 2018 to 2022. This study analyzes spatial and temporal characteristics, employing the Geodetector with optimal parameters to explore the underlying mechanisms. The findings reveal the following: (1) The method achieves an overall accuracy of land use classification surpassing 88.67%, with a Kappa coefficient exceeding 0.87. Specifically, the accuracy for identifying abandoned cropland reaches 87.00%. (2) From 2018 to 2022, the abandonment rate in Mingshan County fluctuated between 4.58% and 5.77%, averaging 5.03%. The lowest abandonment rate occurred in 2019–2020, while the highest was observed in 2020–2021. (3) Cropland abandonment is influenced by both natural and social factors. Elevation and slope are the main driving factors, alongside factors such as distance to road, town, and residential settlement that all significantly contribute to abandonment trends. These five factors exhibit positive correlation with the abandonment rate, with distance to the river showing relatively weaker explanatory power.

**Keywords:** abandoned cropland; hilly; Google Earth Engine; Mingshan County; China



**Citation:** Wei, Y.; Wen, J.; Zhou, Q.; Zhang, Y.; Dong, G. Mapping Cropland Abandonment in the Cloudy Hilly Regions Surrounding the Southwest Basin of China. *Land* **2024**, *13*, 586. <https://doi.org/10.3390/land13050586>

Academic Editor: Le Yu

Received: 4 April 2024

Revised: 23 April 2024

Accepted: 26 April 2024

Published: 28 April 2024



**Copyright:** © 2024 by the authors. Licensee MDPI, Basel, Switzerland. This article is an open access article distributed under the terms and conditions of the Creative Commons Attribution (CC BY) license (<https://creativecommons.org/licenses/by/4.0/>).

## 1. Introduction

Cropland abandonment is a widespread global phenomenon, posing a serious challenge to rural economies and the stability of the food supply chain [1–4]. Historically, dating back to the 19th century, this trend has primarily been observed in European and developed industrialized countries, notably in Europe [5], the United States of America [6], and East Asia [7]. However, in recent decades, numerous developing countries such as China [8] and Nepal [9] have experienced substantial rates of cropland abandonment. The factors influencing cropland abandonment are diverse, encompassing natural conditions, labor dynamics, levels of agricultural development, geographical factors, economic development levels, and agricultural policies [10,11]. In China, cropland abandonment is prevalent due to factors like complex topography and extensive mountainous regions [12,13], leading to adverse effects on agricultural productivity. Sichuan Province is the only major grain-producing province in western China and one of the 13 major grain-producing provinces in China. At the same time, it is also a populous province and a major province for the transformation of grain consumption, playing an important role in ensuring national food security. However, the majority of cropland is distributed in hilly areas, accounting for

57.6% of the total cropland area in the province. With the development of rural economy and the strengthening of farmers' market awareness, the phenomenon of abandoned farmland is becoming increasingly prominent. In-depth analysis of the current situation of farmland abandonment is not only helpful for the government to further improve relevant policies but also necessary to promote the sustainable and healthy development of agriculture in Sichuan and ensure national food security. Therefore, it is imperative to conduct research on abandoned lands to ensure food security, implement rational land planning, and improve people's livelihoods [14,15].

The spatiotemporal characteristics of abandoned cropland are vital for understanding its causes and ecological impacts, serving as essential information for policy formulation. Hilly terrain, acting as a transitional zone between mountains and plains, is inherently susceptible to cropland abandonment [16–19]. Its rugged topography hinders the use of machinery, complicating the adoption of modern, market-oriented agricultural practices and resulting in small-scale, low-intensity agricultural systems [20]. Simultaneously, the rapid pace of urbanization and population outmigration from rural areas have triggered widespread cropland abandonment in China's hilly and mountainous regions [21]. Previous studies have delved into the spatiotemporal distribution and determining factors of cropland abandonment, revealing that the impact of environmental or socio-economic factors may manifest distinct characteristics depending on the scale [1,12,16]. However, due to the lack of long-term observation data on cropland abandonment, there has been limited research on the extent of abandonment, particularly its spatial distribution, in rural hilly regions of China [16]. Additionally, constrained by terrain conditions, most studies have relied primarily on farmer interviews and field survey data [12,22]. While field surveys offer high precision, they still fall short in reflecting the spatiotemporal patterns of abandonment [23]. To explore the underlying driving factors behind abandonment, researchers have employed various methods, including statistical modeling [24,25], machine learning, and data mining techniques [26]. These methods often treat cropland abandonment observations as independent, but the multi-level structure of abandonment phenomena may lead to potential correlations among observations, exaggerating the significance of certain variables and compromising the accuracy of analysis. Therefore, there is an urgent need to comprehend the spatiotemporal patterns and driving factors of cropland abandonment in China's hilly regions, especially in the hilly areas of the Sichuan Basin where the situation remains unclear.

While monitoring farmland is crucial, mapping the abandonment of agricultural fields is challenging and often lacks regular surveillance [4]. Remote sensing emerges as a highly efficient method for obtaining spatiotemporal information on large-scale abandoned croplands, offering improved accuracy in depicting their distribution compared to traditional farmer surveys [27,28]. The assessment of large-scale abandoned lands primarily relies on low-resolution satellite imagery, such as that provided by MODIS, due to its high temporal resolution and global coverage [29]. Conversely, small-scale abandoned lands are typically mapped using moderate-resolution satellite imagery [30–32]. Nevertheless, the fragmentation of abandoned lands in hilly areas poses a significant challenge, as the resolutions of Landsat and MODIS are inadequate to capture this complexity, leading to errors in delineating fragmented abandoned areas [17]. In addition, atmospheric conditions impact data collection for all-optical remote sensing sensors, leading to significant cloud contamination and diminished image availability [33]. In addressing such hilly terrains, it is imperative to improve the spatiotemporal resolution of remote sensing images to improve their availability and accuracy in identifying abandoned land [17]. The utilization of big data cloud computing platforms like Google Earth Engine (GEE) [13,34] has proved effective in managing satellite data ranging from medium to high resolution, thereby enhancing the efficiency of acquiring extensive timeseries datasets. Sentinel-2 images, renowned for their high spatial and temporal resolution, have been widely used for land use and cover change analysis. Similarly, Sentinel-1 images, providing high-resolution imagery unaffected by weather conditions, are extensively utilized for land cover classification

and crop mapping [35,36]. However, research focusing on extracting abandoned land based on Sentinel-1 and Sentinel-2 images remains limited. Therefore, integrating Landsat 8, Sentinel-2, and Sentinel-1 data presents a viable and logical approach to obtaining a more accurate spatiotemporal distribution of abandoned land, particularly in hilly areas characterized by fragmented land and significant cloud interference.

In this study, abandoned cropland is defined as “cropland that has been left fallow or uncultivated for a duration of one year or longer, considering the specific conditions of the study area and available data sources”. The primary objectives of this research are twofold. Firstly, the aim is to develop a cropland abandonment map in the hilly regions surrounding the southwestern basin using multi-source satellite imagery. Secondly, the goal is to determine the abandonment rate of cropland in Mingshan County, China, along with its driving factors, taking into consideration natural and social factors. Three specific research questions have been formulated:

1. How can we accurately create a cropland abandonment map in the hilly regions surrounding the southwestern basin using a time series of optical satellite images?
2. Can Landsat 8, Sentinel-2, and Sentinel-1 imagery contribute to identifying cropland abandonment in areas prone to cloud cover and fragmented land parcels?
3. What spatiotemporal pattern characterizes cropland abandonment in the study area, and what are the influencing factors?

## 2. Materials and Methods

### 2.1. Study Area

Mingshan County is located within Ya'an City, Sichuan Province, situated on the southwestern periphery of the Sichuan Basin and Chengdu Plain. Geographically, its coordinates range from 103°02' to 103°23' east longitude and 29°58' to 30°16' north latitude, encompassing a total area of 614 square kilometers (Figure 1). This area lies within the mid-latitude inland region, characterized by distinct seasons. The terrain varies, with higher elevations in the northwest and lower elevations in the southeast, predominantly featuring terraced hills and shallow hillsides.

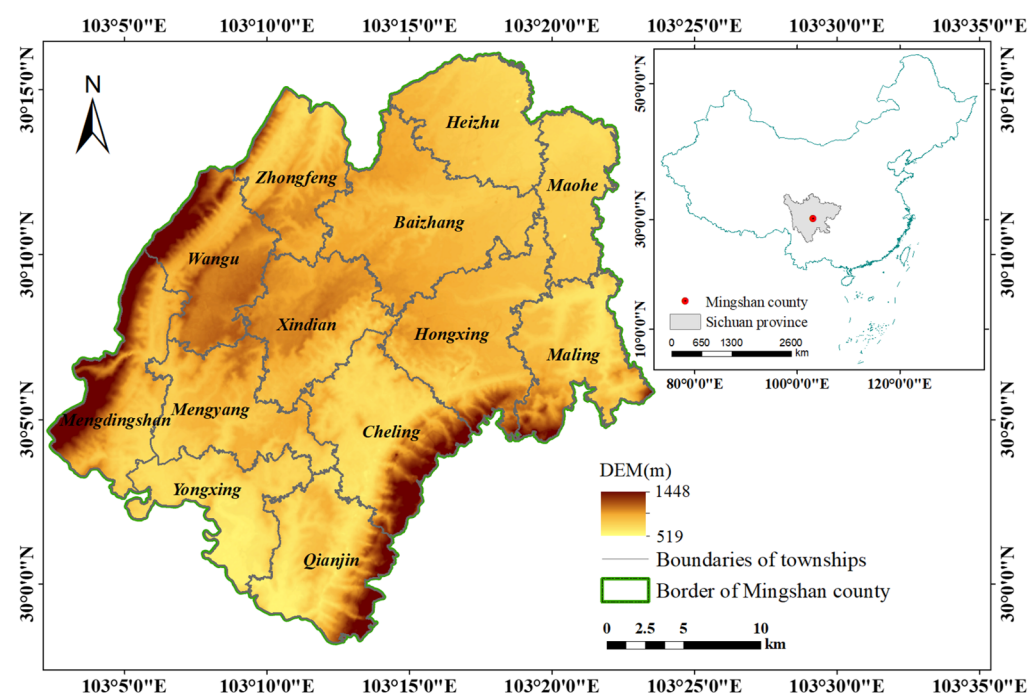


Figure 1. An overview map of the study area.

The region holds significant agricultural importance due to its abundant resources, with a cultivated area of 162,700 hectares dedicated to cereal crops. Its total output amounts to 67,900 tons, including major crops such as rice, wheat, corn, rapeseed, and tea. Recognized as the “granary” of Ya’an, it serves as a primary production area for grains and oils, establishing itself as one of the key commodity grain bases in the province. This region epitomizes the characteristics of a hilly agricultural county situated on the edge of a basin.

## 2.2. Data Source

The remote sensing data utilized in this study included Sentinel-2 MSI and Sentinel-1 SAR with a spatial resolution of 10 m, obtained from the Google Earth Engine (GEE) platform for the period of 2018–2022, as well as Landsat 8 Tier 1 with a spatial resolution of 30 m (Table 1). Elevation data with a spatial resolution of 30 m were retrieved from the Shuttle Radar Topography Mission (SRTM) via the GEE platform. Auxiliary data sources encompassed Google Earth images, the European Space Agency (ESA) World Cover 2020 land cover dataset [37], and the global ESRI 2020 land cover dataset [38], which are all accessible through the GEE platform. Additionally, this study employed the Global Land Cover Fine Classification System (GLC\_FCS30) [39] and the China Annual Land Cover Dataset (CLCD) [40]. Training and validation samples for pre-classification were selected using auxiliary data and compared with the classification results obtained through the proposed method.

**Table 1.** Satellite imagery used in this study.

| Product             | Satellites          | Temporal Resolution | Spatial Resolution | Selected Bands | Level of Correction |
|---------------------|---------------------|---------------------|--------------------|----------------|---------------------|
| Sentinel-1 SAR, IW  | Sentinel-1A and -1B | 6 days              | 10 m               | VV and VH      | GRD                 |
| Sentinel-2 MSI, L1A | Sentinel-2A and -2B | 5 days              | 10–20 m            | VNIR and SWIR  | TOA                 |
| Landsat 8 Tier 1    | Landsat 8           | 16 days             | 30 m               | VNIR and SWIR  | TOA                 |

The administrative boundaries of Mingshan County and its township-level divisions were derived from the 2021 national 1:1,000,000-scale vector boundary dataset. Data regarding towns, roads, and rivers were obtained from the 2021 National Geographic Information Resource Catalog Service System, specifically from the 1:1,000,000 public version of basic geographic information data. Resident point data were determined by collecting latitude and longitude coordinates for each administrative village and subsequently mapping their spatial distribution using ArcGIS.

## 2.3. Mapping the Multi-Year Trajectory of Cropland Abandonment

For the first research question (“How can we accurately create a cropland abandonment map in the hilly regions surrounding the southwestern basin using a long time series of optical satellite images?”), a framework was developed for constructing such a map. This framework comprises five primary components (Figure 2): data collection and preprocessing, generation of training data, annual land cover classification, multi-year cropland abandonment mapping, and accuracy validation.

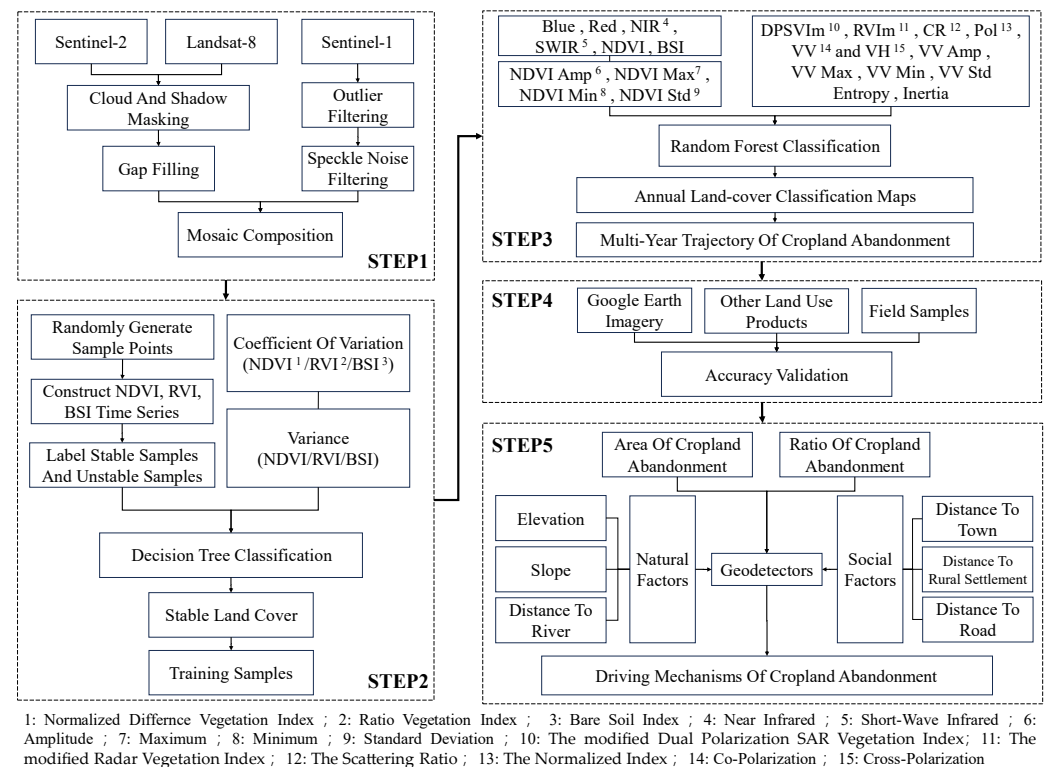


**Figure 2.** Flow chart of this study.

### 2.3.1. Data Preprocessing

To address the second research question (“Can Landsat 8, Sentinel-2, and Sentinel-1 imagery contribute to identifying cropland abandonment in areas prone to cloud cover and fragmented land parcels?”), land use classification maps were generated spanning from 2018 to 2022 using data from Landsat 8, Sentinel-2, and Sentinel-1. This initiative aimed to facilitate the identification of various patterns of cropland abandonment in cloud-prone hilly areas. The preprocessing of the land cover classification data primarily consisted of two main parts.

The first part involved preprocessing the Sentinel-2 and Landsat 8 time series, which encompasses several steps. Firstly, cloud and shadow cover in Sentinel-2 MSI and Landsat 8 OLI images were masked using QA (data product quality assessment) bands. Subsequently, additional cloud masking in the Sentinel-2 MSI images was performed by applying thresholds on the visible, near-infrared, and shortwave infrared bands. Following the cloud masking process, the time series for Sentinel-2 MSI and Landsat 8 OLI were independently synthesized. The Landsat 8 time series was then calibrated to align the reflectance values with those of Sentinel-2 and merged with the Sentinel-2 data. Furthermore, to match the resolution of Sentinel-2, the Landsat images were resampled to 10 m using the GEE nearest neighbor resampled method. When the various optical sensors provided cloud-free pixels at a specific location and time, priority was given to pixels with the highest values [41]. Landsat data were only used to fill gaps in the cloud cover between the Sentinel-2 time series [42,43]. The Sentinel-2 images used for each optical image synthesis cover 85–95% of the study area, ensuring high accuracy in the subsequent classification processes. Monthly summary metrics were gathered, including values for the blue, red, NIR, SWIR bands, NDVI, and BSI (Table 2). Additionally, annual spectral–temporal indicators for the NDVI time series, including minimum, maximum, amplitude, and standard deviation, were computed.

The second part involved preprocessing the Sentinel-1 time series. Firstly, the VV and VH annual time series of Sentinel-1 were merged and synthesized into 12-month composite sequences of VV and VH [42]. Subsequently, the time series was condensed

to monthly intervals using average reflectance values to reduce speckle and noise [44,45]. The resulting 12-month SAR time series serves as the basis for calculating radar seasonal indices. Various radar vegetation indices, including the modified Dual Polarization SAR Vegetation Index (DPSVIm), the Scattering Ratio (CR), the Normalized Index (Pol), and the modified Radar Vegetation Index (RVIm), were computed (Table 2). Haralick techniques were then employed to calculate entropy and inertia (from the “Gray-Level Co-occurrence Matrix”) texture metrics for each  $5 \times 5$  pixel in the VV and VH monthly composite material within the GEE platform [44].

**Table 2.** Optical and SAR indices and their expressions used in this study.

| Indices  | Expressions   | Citations |
|--|---|-----------|
| The modified Dual Polarization SAR Vegetation Index (DPSVIm) | $DPSVIm = \frac{VV+VV \cdot VH}{\sqrt{2}}$                  | [46]      |
| The Scattering Ratio (CR)                                    | $CR = \frac{VV}{VH}$  | [47]      |
| The Normalized Index (Pol)                                   | $Pol = \frac{VH-VV}{VH+VV}$                                 | [48]      |
| The modified Radar Vegetation Index (RVIm)                   | $RVIm = \frac{4VH}{VH+VV}$                                  | [49]      |
| Normalized Difference Vegetation Index (NDVI)                | $NDVI = \frac{NIR-Red}{NIR+Red}$                            | [50]      |
| Ratio Vegetation Index (RVI)                                 | $RVI = \frac{NIR}{Red}$                                     | [51]      |
| Bare Soil Index (BSI)  | $BSI = \frac{(SWIR+Red)-(NIR-Blue)}{(SWIR+Red)+(NIR-Blue)}$ | [52]      |

### 2.3.2. Generate Training Samples

To generate training samples, a decision tree-based method was employed to create a consistent set of land use types, which was subsequently used for land use classification.

The first step involved labeling stable and changing samples of land use types. Initially, numerous random sample points were generated within the study area. Subsequently, the NDVI, RVI, and BSI (Table 2) were computed for each random sample point, and the HANTS harmonic analysis method was applied to smooth their time series. Finally, through time series analysis, whether the temporal curves of random sample points underwent significant changes was observed. This process was used to categorize stable samples (unchanged pixels) (Figure 3b–d) and unstable samples (varying pixels) (Figure 3e–g).

The second step involved identifying stable land use regions. Utilizing labeled sample data representing stable and changing areas and considering variance and the coefficients of variation in the features of NDVI, RVI, and BSI, a decision tree classifier was employed to categorize remote sensing images. This process resulted in the identification of stable land use type regions and changing regions between 2018 and 2022. In the identified stable land use type regions, pixel values consistently fluctuated over time, while changing regions exhibited abrupt variations in pixel.

The third step involved creating a stable land use sample set. This process includes randomly generating a specific number of sample points for different land use categories within stable regions each year in conjunction with existing land use data. Subsequently, the sample point data underwent verification and screening, resulting in the final validated dataset. In this study, the constructed sample set comprises 613 samples of cropland, 400 samples of garden land, 418 samples of shrubland, 500 samples of forest, 214 samples of water bodies, and 419 samples of impervious surfaces, totaling 2564 samples (Figure 3a) (Table 3).

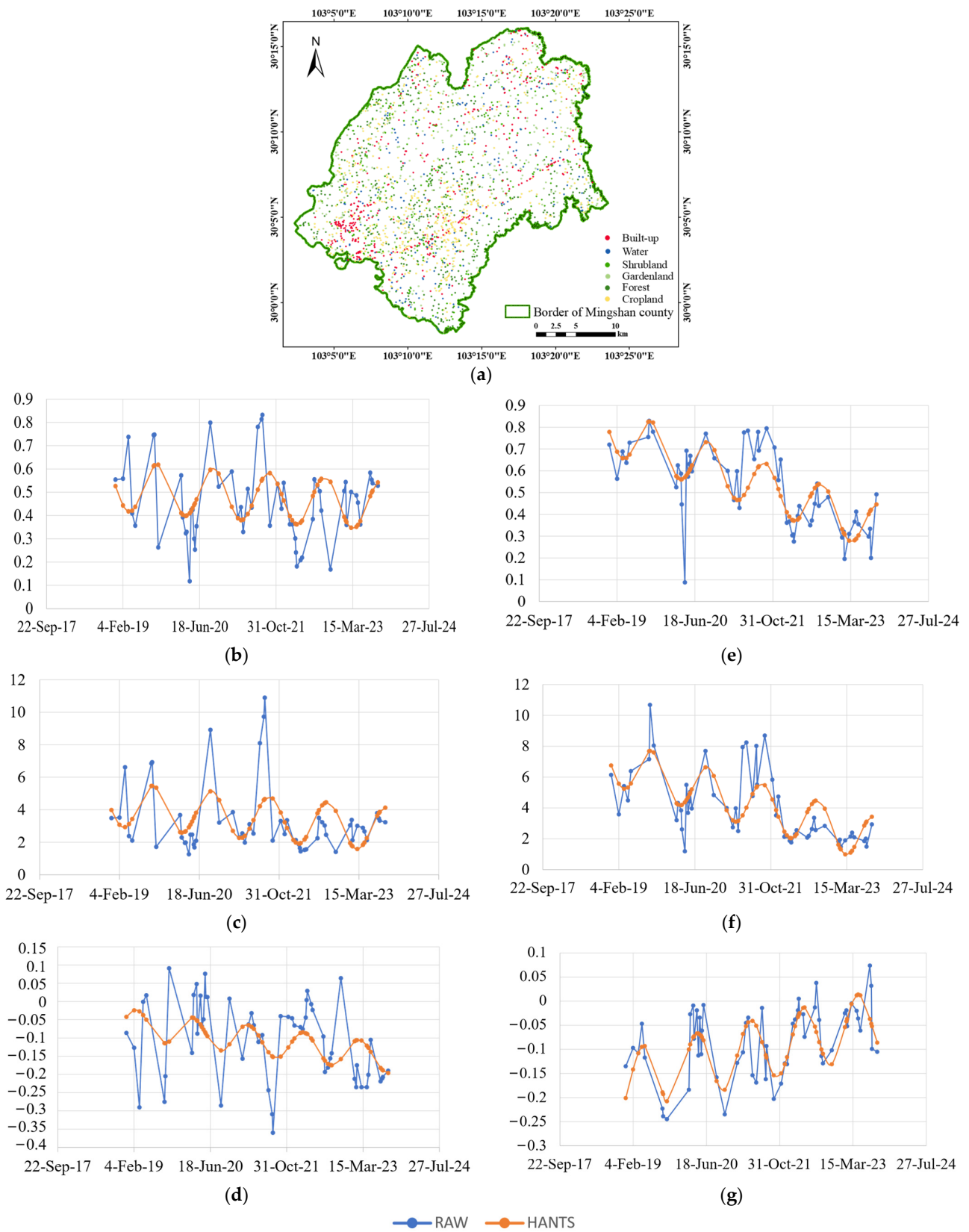


**Figure 3.** (a) The stable sample set comprising different land use types; (b–d) NDVI, RVI, and BSI time series curves of stable samples; (e–g) NDVI, RVI, and BSI time series curves of unstable samples.

**Table 3.** Training samples distributed across land cover classes and years.

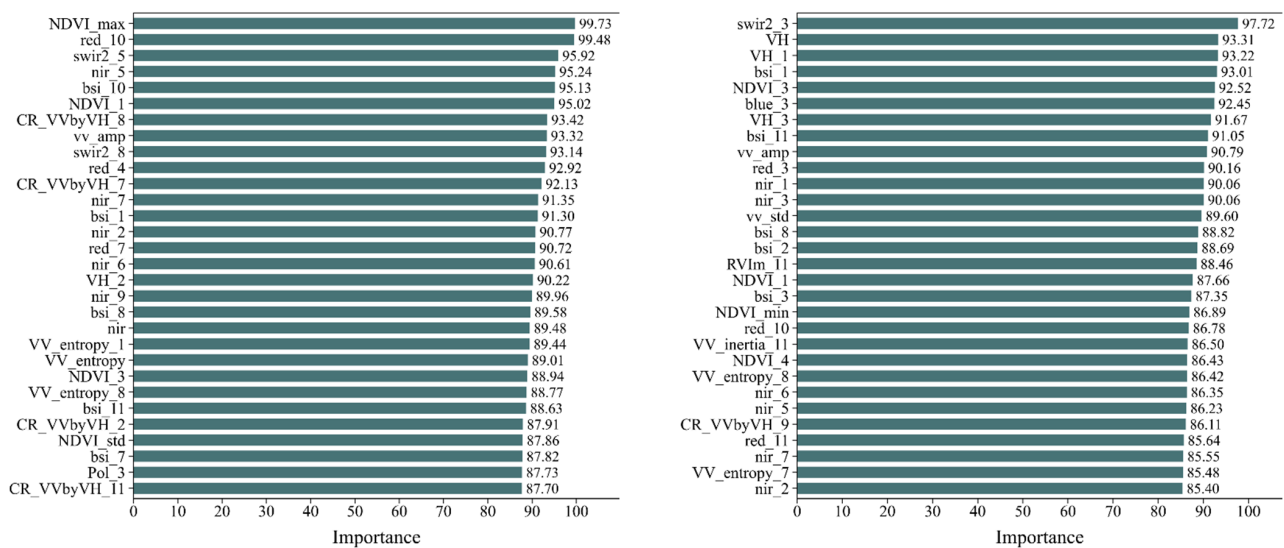
| Class       | 2018 | 2019 | 2020 | 2021 | 2022 | Combined |
|-------------|------|------|------|------|------|----------|
| Cropland    | 122  | 126  | 121  | 121  | 123  | 613      |
| Garden land | 80   | 80   | 80   | 80   | 80   | 400      |
| Shrubland   | 83   | 85   | 83   | 83   | 84   | 418      |
| Forest      | 100  | 100  | 100  | 100  | 100  | 500      |
| Water       | 42   | 45   | 42   | 43   | 42   | 214      |
| Built-up    | 83   | 86   | 83   | 83   | 84   | 419      |
| Total       | 510  | 522  | 509  | 510  | 513  | 2564     |

2.3.3. Annual Land Cover Classification

To produce land use classification maps spanning from 2018 to 2022, the non-parametric machine learning random forest classifier available in Google Earth Engine (GEE) was employed. After multiple fitting experiments, the number of trees in the random forest was set to 220 to achieve better accuracy. The imagery was categorized into six land cover classes, namely cropland, garden land, shrubland, forest, water bodies, and impervious surfaces. Spectral features, phenological characteristics, polarization features, and texture features were chosen for classification. Google Earth Engine (GEE) provides an “interpretability” feature for the random forest classification algorithm, enabling the evaluation of importance scores for the feature variables involved in classification [53]. In this study, feature selection was conducted to utilize only the 30 top-performing features each year for classification (Figure 4a–e). The trained random forest classifier was utilized to perform annual land use classification for the study area, resulting in land use maps for each year.

2.3.4. Multi-Year Cropland Abandonment Mapping

Cropland abandonment is characterized by the transition of cultivated land from one year to the next, exhibiting no signs of agricultural management in the fallow fields. From a land cover perspective, abandoned cropland may represent the later stages of succession, transitioning from cultivated land to shrubland or forested areas. Therefore, two distinct multi-year cropland abandonment trajectories are depicted: ‘Abandonment to Shrubland’ (transitioning from cropland to shrubland) and ‘Abandonment to Forestland’ (transitioning from cropland to shrubland, ultimately evolving into forests) [27,54,55]. These trajectories are based on the annual land cover maps.



(a)

(d)

**Figure 4.** Cont.

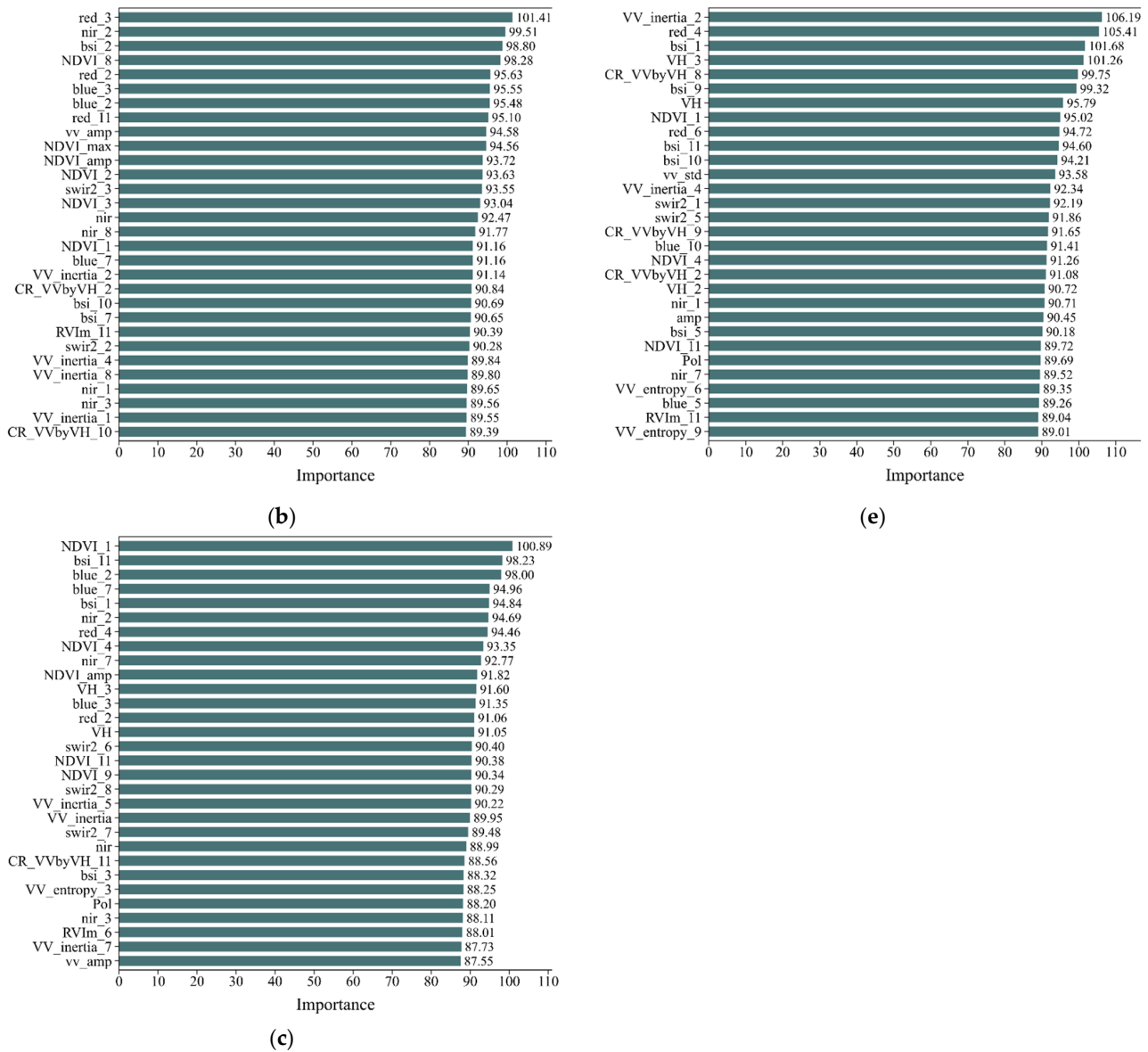


Figure 4. (a–e) Random forest variable importance from 2018 to 2022.

### 2.3.5. Accuracy Validation

The accuracy of the annual land cover maps and cropland abandonment maps was quantified. To assess the accuracy of the annual land cover maps from 2018 to 2022, evaluations were conducted by visually interpreting sentinel multi-seasonal images, other land use products, and high-resolution images available on Google Earth. Each sample was recorded with its corresponding land cover category. Furthermore, 50 sample points were randomly selected from each of the six categories including cropland, garden land, shrubland, forest, water bodies, and impervious surfaces annually, resulting in a total of 300 samples per year. After five years of continuous sampling, we accumulated a total of 1500 sample points. Using these assessment samples, various accuracy evaluation factors were calculated, including overall accuracy (OA), producer’s accuracy (PA), User’s Accuracy (UA), and the Kappa coefficient (KC), using the confusion matrix. The formulas used are as follows:

$$\partial = \frac{\sum_{i=1}^k N_{ii}}{N} \tag{1}$$

$$UA_i = \frac{N_{ii}}{N_{i+}} \tag{2}$$

$$PA_j = \frac{N_{jj}}{N_{+j}} \quad (3)$$

$$Kappa = \frac{N \sum_{i=1}^k N_{ii} - \sum_{i=1}^k (N_{i+} N_{+i})}{N^2 - \sum_{i=1}^k (N_{i+} N_{+i})} \quad (4)$$

where  $N$  signifies the total sample count;  $k$  denotes the total number of columns in the confusion matrix (i.e., the number of categories);  $N_{ii}$  represents the number of samples correctly classified in the  $i$ -th row and  $i$ -th column of the confusion matrix, and the same applies to  $N_{jj}$ ;  $N_{i+}$ , and  $N_{+j}$ , respectively, which represent the total number of samples in the  $i$ -th row and the  $j$ -th column.

To evaluate the accuracy of the cropland abandonment map, and considering the challenges associated with obtaining real-time statistics on abandoned land and acquiring true distribution data for historical years in a long-term time series identification of abandoned land, the results of cropland abandonment extraction for 2021–2022 were verified by using abandoned land samples from on-site investigations conducted in 2022. Accuracy, precision, recall, and F1 were calculated based on the confusion matrix by using the following formulas:

$$\text{Accuracy} = \frac{TP + TN}{TP + FP + TN + FN} \quad (5)$$

$$P = \frac{TP}{TP + FP} \quad (6)$$

$$R = \frac{TP}{TP + FN} \quad (7)$$

$$\frac{1}{F1} = \frac{1}{2} \cdot \left( \frac{1}{P} + \frac{1}{R} \right) \quad (8)$$

where  $TP$  (True Positive),  $FP$  (False Positive),  $TN$  (True Negative), and  $FN$  (False Negative) represent the respective counts of test samples.

#### 2.4. Analysis of the Spatiotemporal Characteristics and Driving Factors of Abandoned Cropland

##### 2.4.1. Analysis of Spatiotemporal Characteristics of Cropland Abandonment

In addressing the third research question (“What spatiotemporal pattern characterizes cropland abandonment in the study area, and what are the influencing factors?”), both spatiotemporal feature analysis and factor analysis were conducted. For spatiotemporal feature analysis, the abandonment rate was calculated annually for each township, as well as the four-year average abandonment rate:

$$P_i = \frac{A_i}{S_i} \times 100\% \quad (9)$$

where  $P_i$  represents the cropland abandonment rate for township  $i$ ,  $A_i$  denotes the cropland abandonment area for township  $i$ , and  $S_i$  is the total cropland area for township  $i$ .

##### 2.4.2. Analysis of Driving Factors of Cropland Abandonment

Geodetectors are a spatial statistical method used to analyze the spatial variability of geographical elements and the relationships among potential driving factors [56]. Within this framework, factor detectors serve as a fundamental component and are capable of discerning whether independent variables act as driving factors for dependent variables, partially explaining the spatial distribution mechanism of the dependent variable. Therefore, in this study, factor detectors were chosen to analyze the driving factors of cropland abandonment, as depicted by the following expression:

$$Q = 1 - \frac{\sum_{h=1}^L N_h \sigma_h^2}{N \sigma^2} \quad (10)$$

where  $Q$  signifies the explanatory power index of the driving factors of cropland abandonment, ranging from  $[0, 1]$ . A higher  $Q$  value indicates the stronger explanatory power of the factor variables for cropland abandonment.  $h$  represents the number of zones or categories,  $N$  and  $N_h$  denote the total number of units in the study area and the number of units in subregion  $h$ , respectively, while  $\sigma^2$  and  $\sigma^2h$  indicate the variance in the dependent variable for the entire region and subregion  $h$ , respectively.

The Optimal Parameter Geographic Detector (OPGD) model was utilized to effectively manage the selection of optimal discretization methods and quantities for the type of data, thereby minimizing the influence of subjective factors [57]. After optimizing the data discretization, factor detection was employed to conduct a driver factor analysis of cropland abandonment in hilly areas. The implementation of this analysis was carried out using the Geodetector model, which is accessible through the R programming language package (<https://cran.r-project.org/>, accessed on 6 January 2024).

### 3. Results

#### 3.1. Mapping Accuracy

##### 3.1.1. Results of Land Use Classification

By analyzing satellite images from 2018 to 2022, annual land use classifications were obtained (Figure 5a–e) (Table 4). This study reveals that the overall accuracy of land cover types for each period exceeded 88.67%, with an average Kappa coefficient of 0.87. Notably, both the user accuracy (UA) and producer accuracy (PA) for cropland classification in each period surpassed 88%, peaking in 2021, where UA and PA reached 91.92% and 92.44%, respectively (Table 5). However, the average PA and UA values for garden land were relatively lower, at 88.33% and 84.62%, respectively. PA and UA reached values of 89.43% and 88.68% for shrubland, and 87.18% and 91.36% for forest. The classification accuracy for water was the highest, with average PA and UA values of 94.68% and 95.31%, respectively. Finally, the PA and UA for impervious surfaces were 90.27% and 89.48%, respectively.

**Table 4.** The proportion of each land use class area in Mingshan County from 2018 to 2022.

| Class       | Area (%) |       |       |       |       |
|-------------|----------|-------|-------|-------|-------|
|             | 2018     | 2019  | 2020  | 2021  | 2022  |
| Cropland    | 20.29    | 19.41 | 19.81 | 19.15 | 20.88 |
| Garden land | 31.37    | 31.26 | 31.25 | 31.29 | 29.65 |
| Shrubland   | 6.81     | 6.85  | 6.68  | 6.64  | 5.86  |
| Forest      | 29.46    | 29.67 | 27.96 | 27.40 | 27.62 |
| Water       | 1.94     | 2.13  | 2.59  | 2.52  | 2.54  |
| Built-up    | 10.13    | 10.68 | 11.71 | 13.01 | 13.46 |

**Table 5.** Land use classification accuracy.

| Class       | 2018  |       | 2019  |       | 2020  |       | 2021  |       | 2022  |       |
|-------------|-------|-------|-------|-------|-------|-------|-------|-------|-------|-------|
|             | UA /% | PA /% |
| Cropland    | 91.19 | 91.74 | 87.34 | 88.11 | 87.87 | 88.61 | 91.92 | 92.44 | 89.61 | 90.25 |
| Garden land | 84.51 | 88.24 | 83.94 | 87.79 | 83.33 | 87.30 | 85.53 | 89.04 | 85.81 | 89.26 |
| Shrubland   | 89.07 | 89.80 | 88.11 | 88.89 | 88.61 | 89.36 | 88.84 | 89.58 | 88.80 | 89.54 |
| Forest      | 91.74 | 87.72 | 90.91 | 86.54 | 89.89 | 85.11 | 92.11 | 88.24 | 92.14 | 88.28 |
| Water       | 95.54 | 94.94 | 95.24 | 94.59 | 94.49 | 93.75 | 95.81 | 95.24 | 95.48 | 94.87 |
| Built-up    | 89.29 | 90.09 | 90.16 | 90.91 | 88.24 | 89.11 | 90.91 | 91.60 | 88.79 | 89.62 |
| OA/%        | 90.46 |       | 89.15 |       | 88.67 |       | 91.02 |       | 90.14 |       |
| Kappa       | 0.88  |       | 0.87  |       | 0.86  |       | 0.89  |       | 0.88  |       |

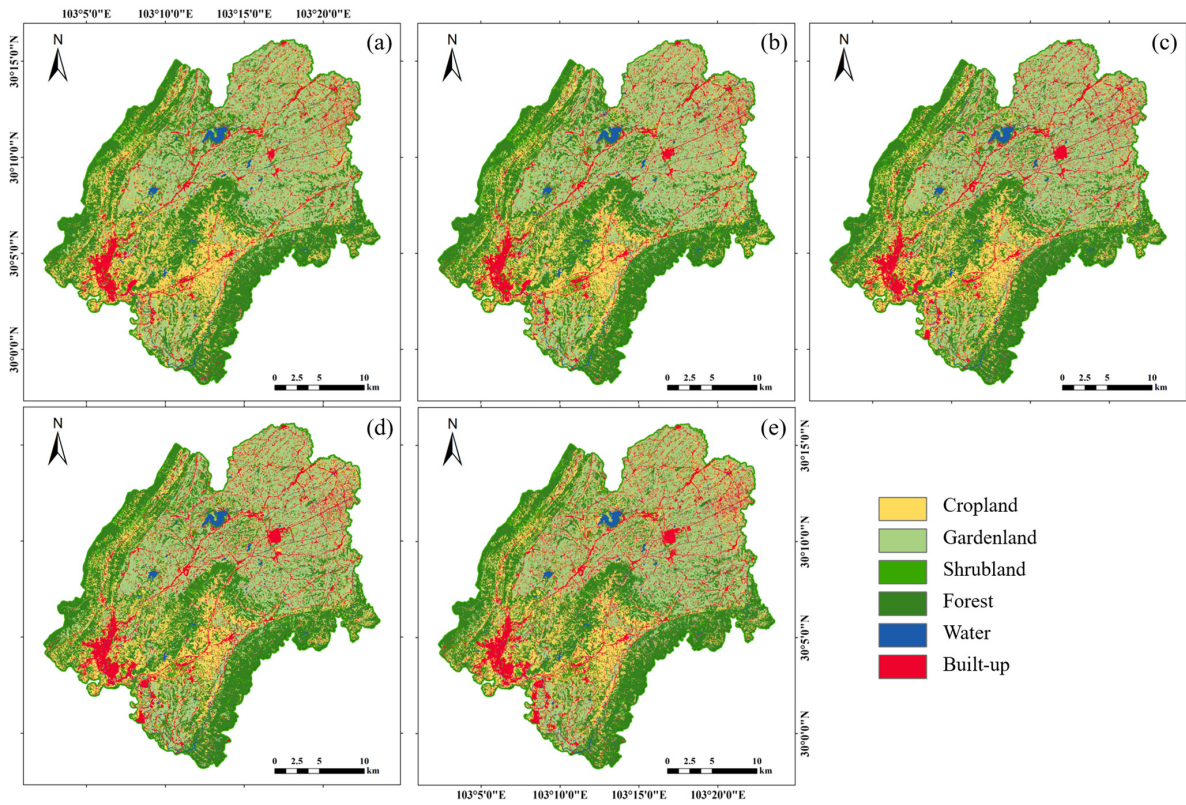


**Figure 5.** (a–e) Results of land use classification in 2018, 2019, 2020, 2021, 2022 in Mingshan County.

To further evaluate the classification results, spatial consistency comparisons were made between high-resolution images available on Google Earth, the global ESRI 2020 land cover dataset, and the classification results of 2020 in this study (Figure 6). Overall, the classification results in this study were significantly superior to those of the global ESRI 2020 land cover dataset.

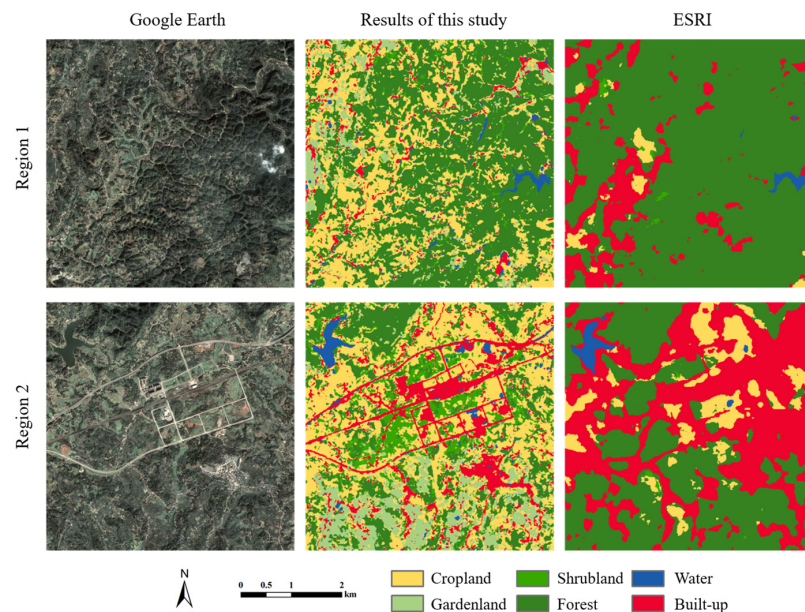


**Figure 6.** Comparison of classification results between this study, the global ESRI 2020 land cover dataset, and high-resolution images available on Google Earth in two regions.

### 3.1.2. Results of Abandoned Cropland Extraction

Field survey data from 2022 yielded 65 sample points for abandoned land and 40 sample points for non-abandoned land (Figure 7). The overall accuracy of abandoned land identification for 2021–2022 was determined to be 0.87, with precision (P) at 0.87, recall (R) at 0.89, and F1 score at 0.88. The monitoring classification maps of cropland abandonment in Mingshan County for the periods 2018–2019, 2019–2020, 2020–2021, and 2021–2022 were derived using the described method (Figure 8).

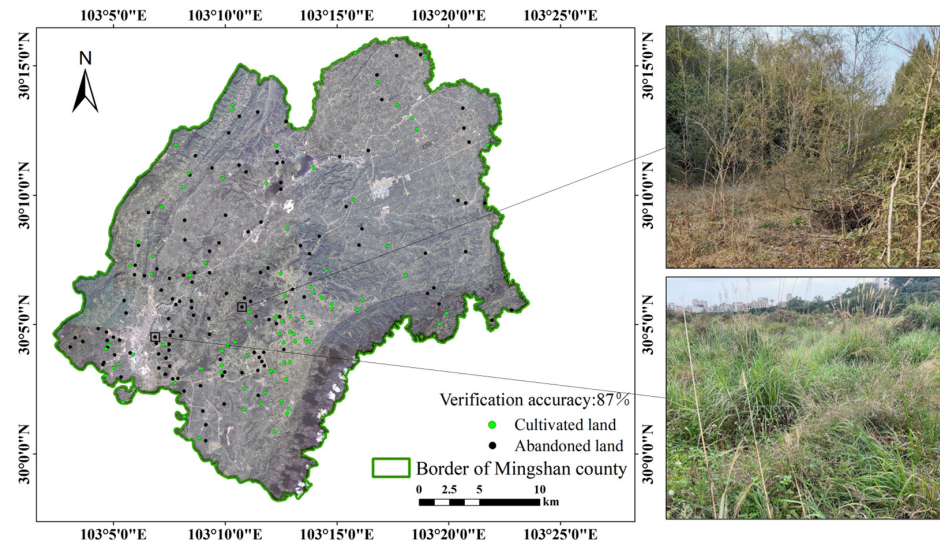


Figure 7. Spatial distribution map and on-site photographs of the 2022 field survey data.

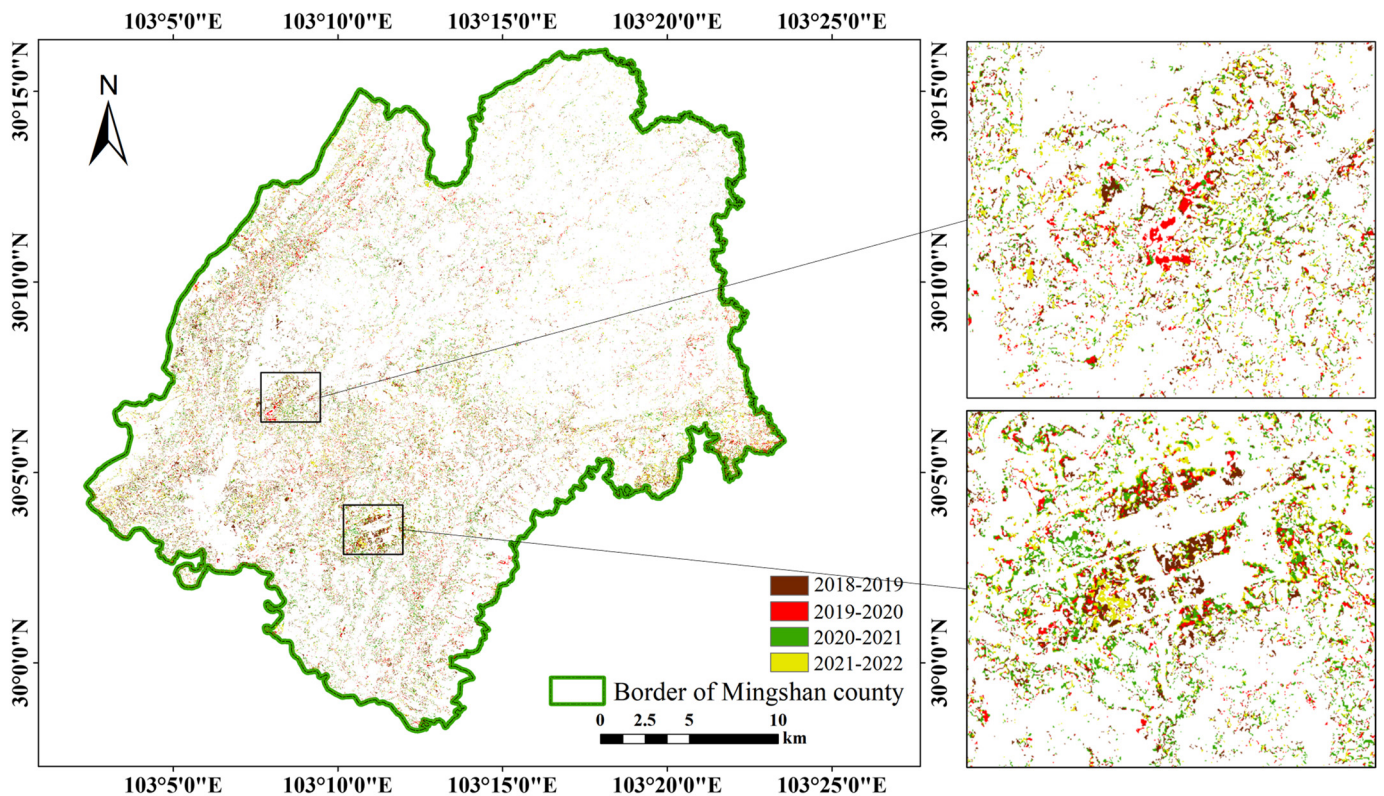
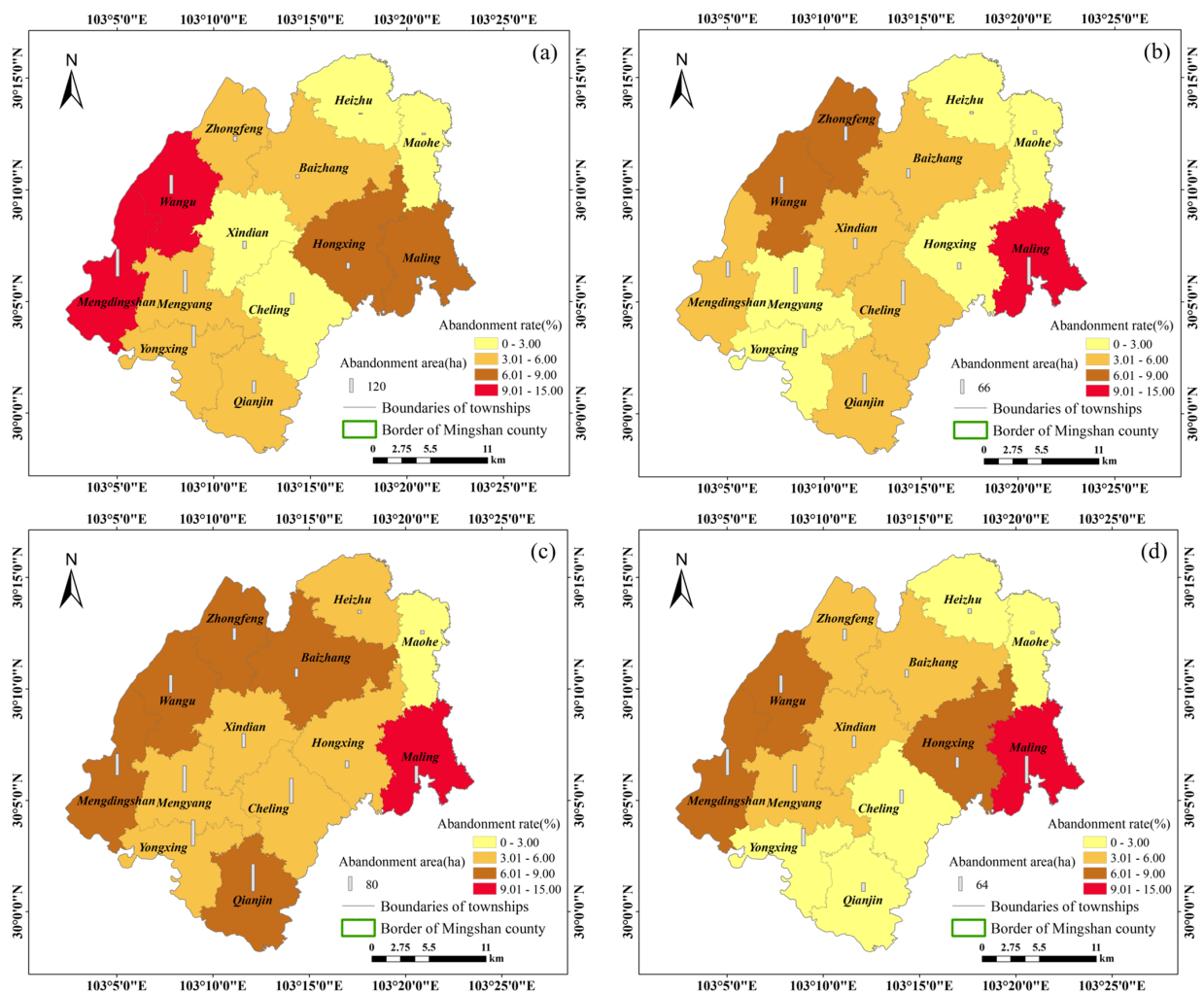


Figure 8. Spatial distribution and local area amplification of abandoned cropland from 2018 to 2022.

### 3.2. Spatiotemporal Characteristics of Cropland Abandonment

#### 3.2.1. Spatial–Temporal Distribution Characteristics of Abandoned Cropland in Various Townships

Concerning abandoned cropland area, in 2018, Mingshan County witnessed 1229.15 hectares of cropland abandonment, primarily concentrated in the southwest region, encompassing Mengdingshan Town, Mengyang Street, Yongxing Street, and Wangu Town (Figure 9a). By 2019, the area of abandoned cultivated land in Mingshan County decreased to 970.72 hectares, marking a 25.09% reduction from the previous period. The distribution shifted, with major abandonment observed in Maling Town, Mengyang Street, and Cheling Town notably moving towards the northeast (Figure 9b). In 2020, the abandoned cultivated land area in Mingshan County increased to 1218.08 hectares, representing an increase of 247.37 hectares compared to the previous phase, with the distribution shifting southeastward, concentrating in Jinjin Town, Mengyang Street, and Yongxing Street (Figure 9c). By 2021, Mingshan County witnessed a decrease in abandoned cultivated land area, totaling only 864.45 hectares, which was mainly found in Maling Town, Mengyang Street, and Mengdingshan Town (Figure 9d). Since 2018, the trend in the abandoned cultivated land area in Mingshan County has shown fluctuations and a downward trajectory. Mengyang Street, Mengdingshan Town, and Yongxing Street have recorded the highest cumulative abandonment area, while Baizhang Town, Maohe Town, and Heizhu Town have seen the least.



**Figure 9.** (a–d) Spatial distribution of abandoned cropland in various townships in 2018–2019, 2019–2020, 2020–2021, and 2021–2022.

In terms of abandonment rates, Mingshan County recorded a rate of 4.93% in 2018, with Mengdingshan Town and Wangu Town experiencing particularly severe rates, both exceeding 10% (Figure 9a). By 2019, the abandonment rate reached its lowest point at 4.58%, and was concentrated spatially in Maling Town, Zhongfeng Town, and Wangu Town (Figure 9b). In 2020, the abandonment rate increased to 5.77%, marking a 1.19% rise from the previous period. Cultivated land abandonment remained concentrated in Maling Town, Wangu Town, and Zhongfeng Town (Figure 9c). By 2021, the abandonment rate decreased to 4.85%, and was down by 0.92% from the previous period, being mainly distributed in Maling Town, Mengdingshan Town, and Wangu Town (Figure 9d). Since 2018, the abandonment rate of cultivated land in Mingshan County has shown a fluctuating trend, with Maling Town, Wangu Town, and Mengdingshan Town exhibiting the highest abandonment rates, while Cheling Town, Heizhu Town, and Maohe Town have recorded the lowest rates.

### 3.2.2. Spatial–Temporal Characteristics of Abandoned Cropland under Different Natural and Social Factors

As elevation increases, the abandoned cropland area initially experiences a rise followed by a decline (Figure 10a). Within the altitude range of 600 to 700 m, the abandoned cropland area reaches its peak, corresponding to a continuous increase in the cropland abandonment rate. Specifically, between 2018 and 2019, areas with elevations exceeding 1000 m witnessed a staggering abandonment rate of 50.09%, highlighting the prevalence of cropland abandonment in high-altitude regions.

Apart from the period between 2018 and 2019, the area of abandoned cropland remained relatively consistent across different slope ranges from 2019 to 2020, 2020 to 2021, and 2021 to 2022, fluctuating between 150 and 200 hectares (Figure 10b). However, the cropland abandonment rate continued to rise, indicating that this phenomenon mainly occurs in steep terrain.

As the distance from the river increases, the abandoned cropland area gradually decreases (Figure 10c). The most concentrated abandoned cropland lies within the range of 0 to 250 m from the river, while the cropland abandonment rate fluctuates, suggesting that the distance from the river has minimal impact on cropland abandonment trends.

The abandoned cropland area decreases with the distance from the road (Figure 10d). It reaches its lowest point within the range of 800 to 1000 m from the road. However, the abandonment rate shows an increasing trend, emphasizing that cropland abandonment mainly occurs in areas far from the road.

As the distance from town increases, the area of abandoned cropland initially rises before declining, mainly concentrated within the range of 2000 to 3000 m (Figure 10e). Concurrently, the cropland abandonment rate displays an upward trajectory, confirming that cropland abandonment primarily occurs in areas distant from the town.

Furthermore, the farther the distance from the rural settlement, the more likely the abandoned cropland area exhibits an initial increase followed by a decrease, and this is mainly concentrated within the range of 800 to 1200 m (Figure 10f). The cropland abandonment rate continues to rise, with the rate of increase accelerating beyond 1600 m, reaffirming that cropland abandonment mainly occurs in areas far from rural settlements.

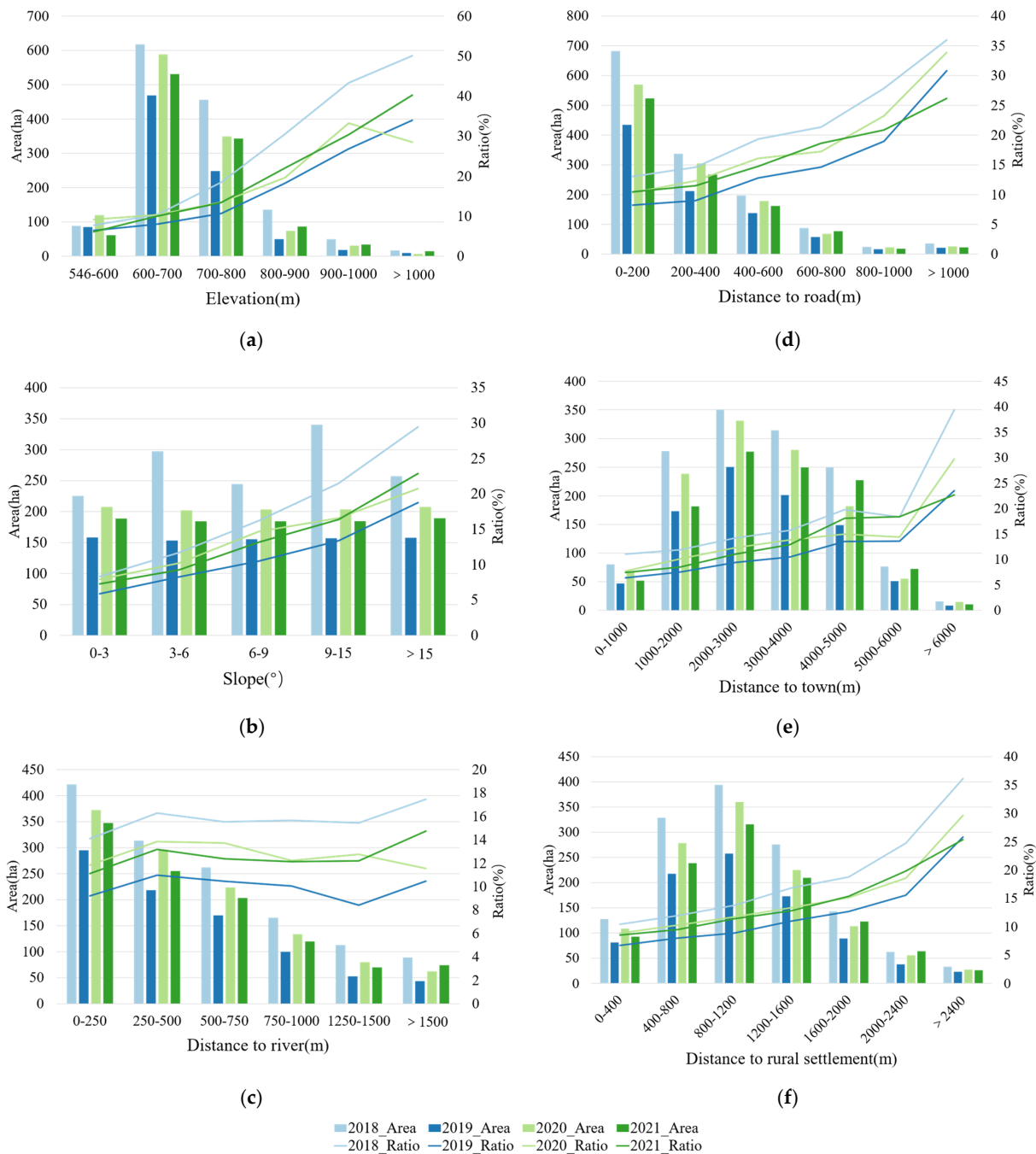


**Figure 10.** (a–f) The relationship between elevation, slope, distance to the nearest river, distance to the nearest road, distance to the nearest town, distance to the nearest rural settlement, and the abandoned cropland area and the ratio of abandoned cropland area within a certain interval to the cropland area in that interval in the Mingshan County from 2018 to 2022.

### 3.3. Driving Factors of Cropland Abandonment

#### 3.3.1. Discretization of Continuous Factors

One notable advantage of the Geodetector module is its ability to derive the optimal ranges of the factors under consideration. This capability is particularly valuable as it aids in identifying the thresholds necessary for subsequently driving factor analyses [58]. The q-value should be calculated for every continuous factor using different grading methods (equidistant grading, natural interval grading, quantile interval grading, geometric interval grading, and standard deviation interval grading) and different numbers of breakpoints.

Moreover, the parameter combination (grading method and number of breakpoints) with the highest q-value should be selected. Since it is preferable to have fewer than eight categories, the number of breakpoints should initially range between three and eight categories. Taking the discretization of abandoned cropland from 2018 to 2019 as an example, when employing the natural interval classification method with eight categories for elevation, the highest q-value is achieved (Figure 11a), thus selecting the natural interval method to categorize elevation into eight categories (Figure 11b). Similarly, the natural interval grading method is selected to divide the slope into seven categories (Figure 11a,b). The discretization approach for other continuous factors follows the same principle.

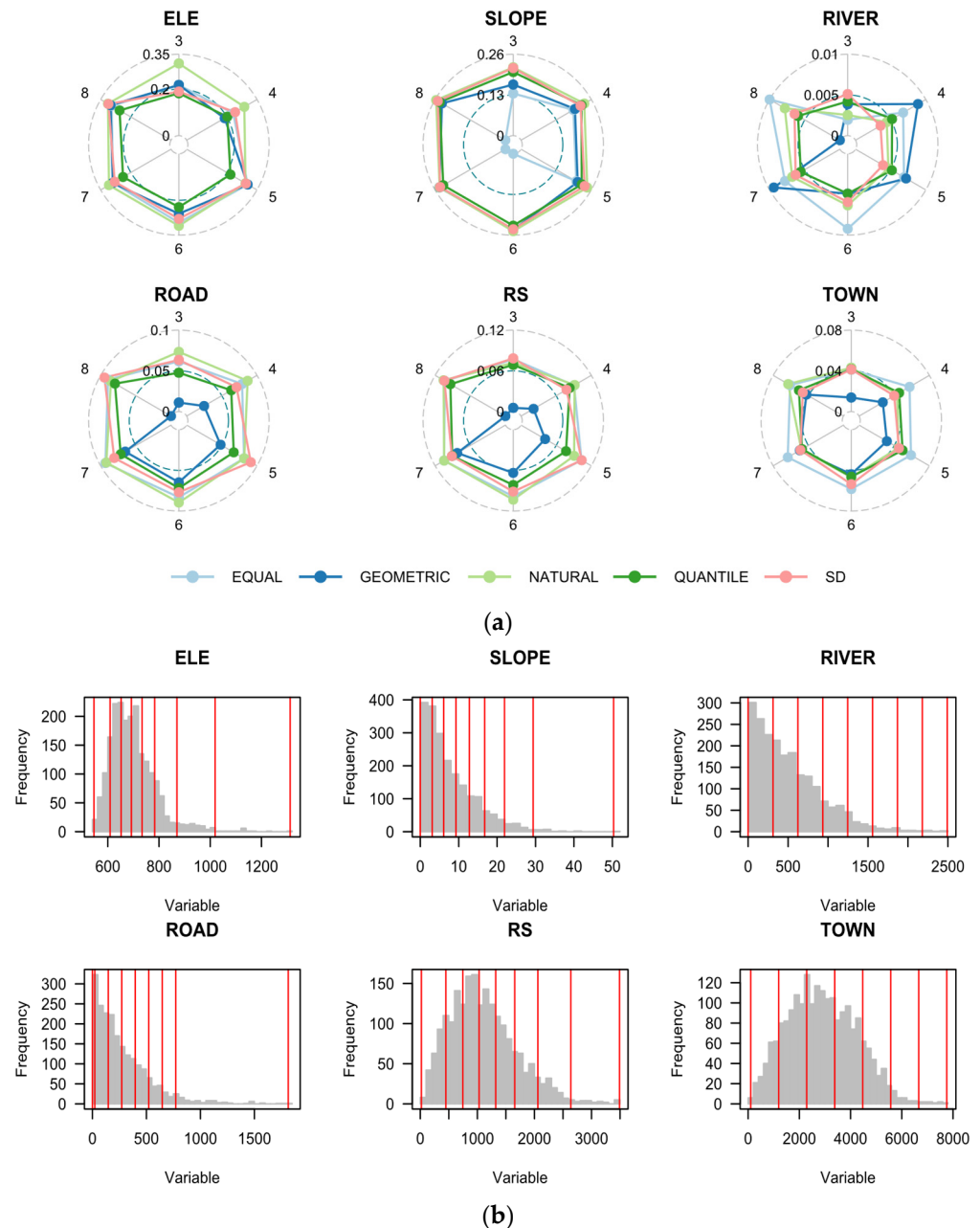


**Figure 11.** (a) Discretization grading method of continuous factors using 2018–2019 abandoned cropland as an example; (b) optimal interval for discretizing continuous factors using 2018–2019 abandoned cropland as an example.

### 3.3.2. Single Factor Detection Results

Using the Optimal Parameter Geographic Detector, the explanatory power of individual factors for cropland abandonment was identified (Figure 12a). On average, natural factors exhibited a q-value of 0.1520, while social factors had an average q-value of 0.0979. This suggests a notably stronger explanatory capacity of natural factors compared to social factors.

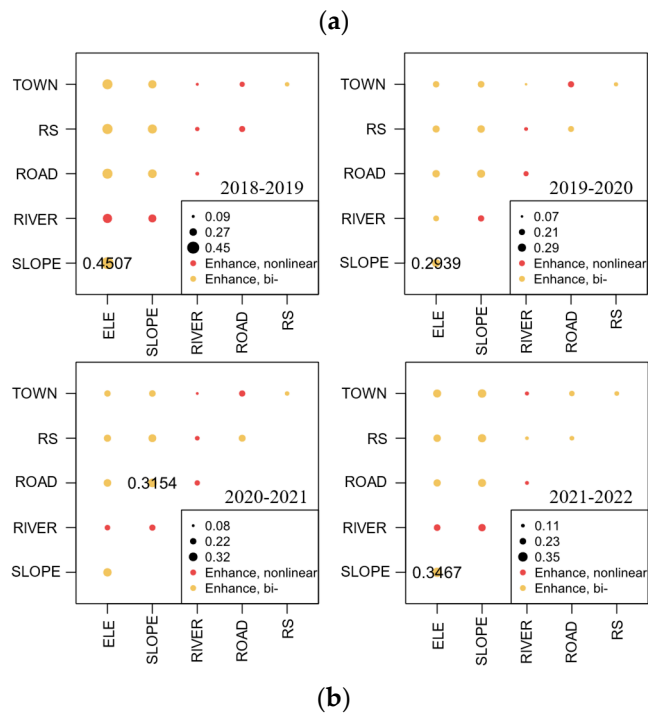
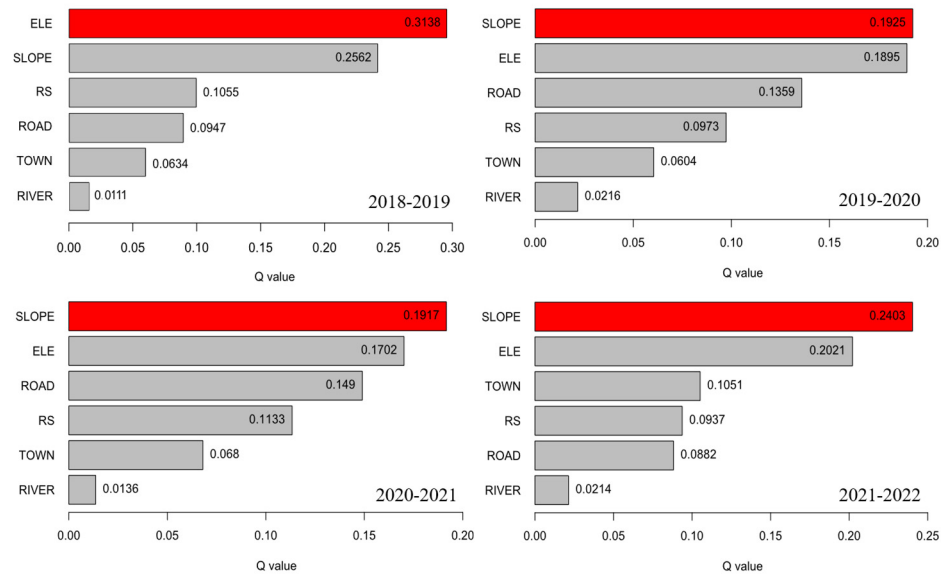


**Figure 12.** (a) Results of factor detection in Geodetector for abandoned cropland from 2018 to 2022; (b) results of interaction detection in Geodetector for abandoned cropland from 2018 to 2022.

Among the natural factors, elevation exhibited the highest explanatory power, followed by slope and distance to the river. Specifically, elevation exhibited the highest explanatory power during the 2018–2019 period, with a q-value of 0.3138. Slope demonstrated relatively high explanatory power in the subsequent periods: 2019–2020, 2020–2021,

and 2021–2022, with values of 0.1925, 0.1917, and 0.2403, respectively. However, the explanatory power of distance to river consistently remained low, with all values below 0.03.

The explanatory power of social factors ranks relatively lower and ranked from highest to lowest as distance to road, rural settlement, and town. The explanatory power of road distance initially increased and then decreased over time. For the period of 2018–2019, the  $q$ -value was 0.0947, which rose to 0.1359 in 2019–2020, peaked at 0.1490 in 2020–2021, and then decreased to 0.0882 in 2021–2022. The  $q$ -values for distance to town fluctuated between 0.0604 and 0.1051, while those for distance to rural settlement remained relatively stable, ranging from 0.0937 to 0.1133.

The explanatory power ( $p$ -values) of all factors was below 0.01, indicating significant detection results. The analysis indicates that slope and elevation exert a predominant influence on cropland abandonment in Mingshan County, while the distance from the road, rural settlement, and the town also hold significant importance. However, the influence of distance to the river appears to be relatively weak.

### 3.3.3. Interaction Detection Results

Based on single-factor detection, interaction analysis was conducted for six factors (Figure 12b). Under interaction, the influence of each factor on cropland abandonment significantly intensifies, with  $q$ -values ranging from 0.0693 to 0.4507, indicating both bi-factor enhancement and non-linear enhancement.

The interaction among different natural factors is particularly noteworthy. During the period of 2018–2019, the interaction between elevation and slope exhibited the strongest explanatory power, with a  $q$ -value of 0.4507, indicating that these two factors combined can account for 45.07% of cropland abandonment. Similarly, for the periods of 2019–2020 and 2021–2022, the interaction between elevation and slope remained prominent, with values of 0.2939 and 0.3467, respectively, indicating their significant role in explaining cropland abandonment.

The interaction between different social factors appears to be relatively subdued. Notably, during the period of 2020–2021, the interaction between distance to road and slope, along with the distance to rural settlement, exhibited the strongest explanatory power, with a  $q$ -value of 0.2462. This value surpassed the explanatory power of distance to road and rural settlement when all were considered as individual factors.

Furthermore, in the interaction between natural and social factors, the interaction of each social factor with elevation and slope emerged as the most significant, surpassing the individual effects of each social factor. The  $q$ -values ranged from 0.378 to 0.511, indicating significant enhancement. During the period of 2018–2019, the interaction between distance to rural settlement and elevation was the most significant, with a  $q$ -value of 0.3784, indicating bi-factor enhancement.

The findings from interaction analysis indicate that while the impact of individual social factors on cropland abandonment may not be significant, their interaction with natural factors leads to non-linear enhancement in explanatory power. This indicates that specific social conditions exacerbate cropland abandonment significantly when encountering high elevation and steep slopes.

## 4. Discussion

### 4.1. Mapping Cropland Abandonment in Cloudy Hilly Regions

This study introduces a framework developed for identifying various trajectories and patterns of cropland abandonment within hilly and cloudy areas by utilizing multisource satellite imagery. Taking Mingshan County as an example, cropland abandonment maps were generated based on land cover changes, addressing the first research question. Between 2018 and 2022, Mingshan County exhibited an average abandonment rate of 5.03%, showing a fluctuating trend. Previous studies have confirmed that in environmentally challenging areas, such as hilly and mountainous regions, the phenomenon of cropland abandonment is common [16,23,59], significantly affecting agricultural sustainability. Upon

examination, the overall accuracy of land use classification surpassed 88.67%, with a commendable identification accuracy in abandoned cropland reaching 87.00%. These results indicate that the method employed for extracting abandoned cropland is not only highly rational but also feasible, offering precision and ease of implementation [13]. The dataset derived from multiple remote sensing sources, combining Landsat 8 and Sentinel-2 images, offers a greater abundance of cloud-free pixels compared to using either Landsat 8 or Sentinel-2 images alone [42]. Additionally, by integrating Sentinel-1 radar data with optical vegetation indices, it was possible to effectively mitigate the impact of clouds and cloud shadows across different scales [35]. Consequently, compared to monitoring based on MODIS time series data with resolutions of 250 m and 500 m, the developed method enabled the tracking of multiple cropland abandonment trajectories at finer scales [27,60], thereby contributing to addressing the second research question. At the same time, a method was successfully devised for generating a stable sample set of land use types. This method is based on a small subset of stable sample points that represent different land use categories and are used to generate training data annually. With this approach, coherent, annually updated high-dynamic land use type maps can be produced, eliminating the cumbersome process of manually selecting training data each year. This method improves efficiency and ensures data accuracy, providing strong support for sample collection in large-scale research areas [4]. Furthermore, classification accuracy depends on feature combinations with or without auxiliary data. The utilization of machine learning methods to classify spatial datasets from various sources presents an opportunity to integrate multiple satellite and spatial data, thereby improving the accuracy of cropland abandonment classification [18].

#### 4.2. Spatial–Temporal Characteristics and Driving Factors of Cropland Abandonment

In this study, six major indicators were selected from both natural and social perspectives to analyze the spatiotemporal characteristics of cropland abandonment, addressing the third research question. The results indicate that cropland abandonment tends to occur in areas characterized by high elevation, steep slopes, and distance from roads, towns, and rural settlements. In regions with high altitudes and steep terrain, cropland is more likely to transition into orchards. This shift is primarily driven by the increased operating costs associated with higher elevations and steep slopes, prompting a transition from cropland to orchards with higher economic value [13]. Moreover, as the distance from towns, residential areas, and roads increases, human intervention decreases, rendering cropland more susceptible to abandonment [23].

Utilizing the optimal parameter geographical detector, the driving factors behind cropland abandonment were investigated. The findings underscore the pivotal role of natural elements in shaping the spatial distribution pattern of abandoned cropland, while social factors also contribute significantly to cropland abandonment. Previous studies have also highlighted the intertwined effects of economic and environmental factors on abandoned farmland [60,61]. Factors like elevation and slope serve as prerequisites for the spatial distribution of cropland. Past research has suggested that elevation and slope may act as limiting factors for mechanization in mountainous areas, contributing to cropland abandonment [22,55]. Additionally, social factors such as the distance to roads, towns, and rural settlements significantly influence the phenomenon of abandoned farmland. This observation confirms findings from other studies, which have noted cropland abandonment in regions with poor agricultural production conditions and inadequate infrastructure [9,61,62]. The abandonment rate fluctuates with the distance from the river. However, prior research has indicated that irrigation, as a crucial aspect of agricultural production, can significantly enhance grain yields [63]. This effect is likely due to the humid and rainy climate in the Ya'an area, where water resources may not solely depend on rivers but also on natural rainfall or channel irrigation. Therefore, being farther away from rivers does not necessarily lead to easier abandonment. Previous studies have predominantly relied on static data types to analyze social factors. However, such approaches can only explore

the static spatial distribution driving force and fail to directly reflect changing driving factors [64]. In contrast, this study incorporates dynamic distance-based social data into the analysis, explaining the differences in cropland abandonment across different stages using evolving social data. An important future direction for this research involves continuously optimizing and refining the established indicator system of driving factors while exploring the underlying mechanisms from a multi-stakeholder perspective [65,66]. This approach will facilitate more meticulous and precise analysis at the micro-level, further validating the findings of this study and providing firmer theoretical support and practical guidance for the development of related fields.

#### *4.3. Policy Implications*

Initially, in response to the phenomenon of cropland abandonment, the government and relevant departments should implement proactive and effective measures, particularly targeting areas with high elevation and steep slopes. This includes implementing land governance projects, advancing terrace construction to address slope issues, constructing high-standard cropland, and organizing land consolidation efforts to merge scattered plots, providing robust support for mechanized agricultural production [67,68]. For cropland with steep slopes, the government should take active measures, implementing policies for retiring cropland and reforestation to effectively prevent soil erosion.

Subsequently, when formulating land use policies, the government should consider geographic factors. Distance from roads, towns, and rural settlement significantly influences cropland abandonment, highlighting the need to consider the rationality and sustainability of land use in planning and development processes. Priority should be given to locating cropland within a reasonable distance from roads, towns, and rural settlement to ensure farmers can conveniently engage in agricultural production and sales [18]. Planning should balance the needs of agricultural development and urban–rural construction, avoiding excessive distance between cropland and towns or rural settlement to reduce farmers' transportation and living costs. Furthermore, efforts should be made to improve rural transportation networks to lower transportation costs for agricultural products and enhance farmers' economic benefits.

Additionally, the protection and management of rivers cannot be ignored, especially those closely related to agricultural production. Despite the relatively weak explanatory power of distance from rivers on abandonment rates according to the findings of this study, the risks of river water pollution and overuse must be intensely considered [63]. These potential issues may adversely affect agricultural production and land use. Therefore, the government should take effective measures to safeguard river ecosystems, maintain stable water supplies, and thus support the sustainable development of agriculture and land use.

#### *4.4. Limitations and Future Research Perspectives*

Firstly, the variability in the definitions of cropland abandonment significantly affects the identification results [13,16,18,69]. There is no uniform standard for defining abandoned cropland, as scholars have different definitions for abandoned cropland in different study areas. Existing definitions of abandonment include “land left fallow for more than one year”, “land left fallow for one season or more”, and “land left uncultivated for two years or more”. Additionally, due to the launch of the Sentinel-2 satellite in 2017, the time span of this study is relatively short, limiting the ability to conduct long-term monitoring of land cover changes. Therefore, based on the actual conditions of the study area and data sources, this study defines abandoned cropland as “cropland left fallow or uncultivated for one year or more (including one year)”. In the future, methods for identifying quarterly, annual, and multi-year abandonment can be further explored based on the determination of whether cropland is abandoned.

Secondly, the accuracy of land classification can result in error propagation [16,69]. Due to the complexity of cropland abandonment phenomena, it is challenging to directly identify abandoned land through remote sensing imagery. This study employs change

detection in land use between adjacent years to extract the distribution of abandoned cropland. However, classification errors inherent in remote sensing imagery can propagate into the extraction of abandoned cropland, leading to inaccuracies. These errors are difficult to eliminate and can only be mitigated by improving the classification accuracy of remote sensing imagery to reduce errors in the extraction of abandoned cropland. In the future, we will utilize higher-resolution images and deep learning methods to better understand agricultural changes within each pixel, thereby enhancing the precision and accuracy of assessments [18].

Lastly, this study did not comprehensively explore the driving factors behind cropland abandonment. Cropland abandonment is influenced by a multitude of factors, including natural, demographic, socio-economic, and policy factors [69]. While this study integrated multiple factors and utilized Geodetectors to investigate the causes of abandonment, the spatiotemporal characteristics of abandonment are also influenced by household-level and policy predictors directly related to farmer decision making. To accurately identify the immediate causes of abandonment, future research should conduct in-depth analyses and collect variables from household-level data.

## 5. Conclusions

Using Google Earth Engine (GEE) and the random forest algorithm, this study proposes a method that integrates multi-source data from Landsat 8, Sentinel-2, and Sentinel-1 to generate land use maps covering the hilly and cloudy areas of southwestern China between 2018 and 2022. This method is applied to extract abandoned cropland, providing a framework for mapping abandoned cropland across various hilly areas globally and thereby serving as a reference point for similar initiatives. Furthermore, this research explores the spatiotemporal distribution patterns and underlying mechanisms of cropland abandonment, aiming to offer policy recommendations to decision makers. The key findings are outlined as follows:

First, the method achieves an overall accuracy exceeding 88.67% in land use classification, with a Kappa coefficient exceeding 0.87. The accuracy of identifying abandoned cropland reaches 87.00%. From 2018 to 2022, the abandonment rate in Mingshan County fluctuates between 4.58% and 5.77%, with an average of 5.03%. The lowest abandonment rate occurred in 2019–2020, while the highest was observed in 2020–2021.

Second, within the elevation range of 600 to 700 m, the abandoned cropland area reaches its peak. It maintains relative stability across different slope ranges, ranging between 150 and 200 hectares. Abandoned cropland is most concentrated within 0 to 250 m of river. Conversely, within the 800 to 1000 m range from road, the area of abandoned cropland reaches its lowest point. Additionally, abandoned cropland is mainly concentrated within the 2000 to 3000 m range from town and the 800 to 1200 m range from rural settlements.

Third, cropland abandonment results from both natural and social factors. Elevation and slope are the primary driving factors, while distance to road, town, and rural settlement also play significant roles. The abandonment rate exhibits positive correlation with these five factors, although distance to river shows relatively weaker explanatory power.

**Author Contributions:** Conceptualization, Y.W. and J.W.; methodology, J.W.; software, J.W. and Q.Z.; validation, J.W.; formal analysis, J.W. and Q.Z.; investigation, J.W.; resources, Y.W. and J.W.; data curation, J.W.; writing—original draft preparation, J.W.; writing—review and editing, Y.W., Y.Z. and G.D.; visualization, J.W.; supervision, Y.W.; project administration, Y.W.; funding acquisition, Y.W. All authors have read and agreed to the published version of the manuscript.

**Funding:** This research is supported by the research interest group project of Sichuan Agricultural University Research on Dynamic Monitoring, Mechanisms, and Governance Pathways of Cropland Abandonment in the Context of Building the “Granary of Tianfu” (Project No.: 2023502).

**Data Availability Statement:** The original contributions presented in the study are included in the article, further inquiries can be directed to the corresponding author.

**Acknowledgments:** We express our gratitude to the anonymous reviewers and editors for their professional comments and suggestions.

**Conflicts of Interest:** The authors declare no conflicts of interest.

## References

- Li, S.; Li, X. Global understanding of farmland abandonment: A review and prospects. *J. Geogr. Sci.* **2017**, *27*, 1123–1150. [[CrossRef](#)]
- Kuntz, K.A.; Beaudry, F.; Porter, K.L. Farmers' Perceptions of Agricultural Land Abandonment in Rural Western New York State. *Land* **2018**, *7*, 128. [[CrossRef](#)]
- Renwick, A.; Jansson, T.; Verburg, P.H.; Revoredo-Giha, C.; Britz, W.; Gocht, A.; McCracken, D. Policy reform and agricultural land abandonment in the EU. *Land Use Policy* **2013**, *30*, 446–457. [[CrossRef](#)]
- Yin, H.; Brandão, A.; Buchner, J.; Helmers, D.; Iuliano, B.G.; Kimambo, N.E.; Lewińska, K.E.; Razenkova, E.; Rizayeva, A.; Rogova, N.; et al. Monitoring cropland abandonment with Landsat time series. *Remote Sens. Environ.* **2020**, *246*, 111873. [[CrossRef](#)]
- Hatna, E.; Bakker, M.M. Abandonment and Expansion of Arable Land in Europe. *Ecosystems* **2011**, *14*, 720–731. [[CrossRef](#)]
- Brown, D.G.; Johnson, K.M.; Loveland, T.R.; Theobald, D.M. RURAL LAND-USE TRENDS IN THE CONTERMINOUS UNITED STATES, 1950–2000. *Ecol. Appl.* **2005**, *15*, 1851–1863. [[CrossRef](#)]
- Su, G.; Okahashi, H.; Chen, L. Spatial Pattern of Farmland Abandonment in Japan: Identification and Determinants. *Sustainability* **2018**, *10*, 3676. [[CrossRef](#)]
- Wang, C.; Gao, Q.; Wang, X.; Yu, M. Decadal Trend in Agricultural Abandonment and Woodland Expansion in an Agro-Pastoral Transition Band in Northern China. *PLoS ONE* **2015**, *10*, e0142113. [[CrossRef](#)] [[PubMed](#)]
- Chaudhary, S.; Wang, Y.; Dixit, A.M.; Khanal, N.R.; Xu, P.; Fu, B.; Yan, K.; Liu, Q.; Lu, Y.; Li, M. A Synopsis of Farmland Abandonment and Its Driving Factors in Nepal. *Land* **2020**, *9*, 84. [[CrossRef](#)]
- Baumann, M.; Kuemmerle, T.; Elbakidze, M.; Ozdogan, M.; Radeloff, V.C.; Keuler, N.S.; Prishchepov, A.V.; Kruhlov, I.; Hostert, P. Patterns and drivers of post-socialist farmland abandonment in Western Ukraine. *Land Use Policy* **2011**, *28*, 552–562. [[CrossRef](#)]
- Lambin, E.F.; Meyfroidt, P. Land use transitions: Socio-ecological feedback versus socio-economic change. *Land Use Policy* **2010**, *27*, 108–118. [[CrossRef](#)]
- Zhang, Y.; Li, X.; Song, W. Determinants of cropland abandonment at the parcel, household and village levels in mountain areas of China: A multi-level analysis. *Land Use Policy* **2014**, *41*, 186–192. [[CrossRef](#)]
- Wang, Y.; Song, W. Mapping Abandoned Cropland Changes in the Hilly and Gully Region of the Loess Plateau in China. *Land* **2021**, *10*, 1341. [[CrossRef](#)]
- Knoke, T.; Calvas, B.; Moreno, S.O.; Onyekwelu, J.C.; Griess, V.C. Food production and climate protection—What abandoned lands can do to preserve natural forests. *Glob. Environ. Chang.* **2013**, *23*, 1064–1072. [[CrossRef](#)]
- Raj Khanal, N.; Watanabe, T. Abandonment of Agricultural Land and Its Consequences. *Mt. Res. Dev.* **2006**, *26*, 32–40. [[CrossRef](#)]
- Han, Z.; Song, W. Spatiotemporal variations in cropland abandonment in the Guizhou–Guangxi karst mountain area, China. *J. Clean. Prod.* **2019**, *238*, 117888. [[CrossRef](#)]
- He, S.; Shao, H.; Xian, W.; Zhang, S.; Zhong, J.; Qi, J. Extraction of Abandoned Land in Hilly Areas Based on the Spatio-Temporal Fusion of Multi-Source Remote Sensing Images. *Remote Sens.* **2021**, *13*, 3956. [[CrossRef](#)]
- Hong, C.; Prishchepov, A.V.; Jin, X.; Han, B.; Lin, J.; Liu, J.; Ren, J.; Zhou, Y. The role of harmonized Landsat Sentinel-2 (HLS) products to reveal multiple trajectories and determinants of cropland abandonment in subtropical mountainous areas. *J. Environ. Manag.* **2023**, *336*, 117621. [[CrossRef](#)] [[PubMed](#)]
- Xu, F.; Ho, H.C.; Chi, G.; Wang, Z. Abandoned rural residential land: Using machine learning techniques to identify rural residential land vulnerable to be abandoned in mountainous areas. *Habitat Int.* **2019**, *84*, 43–56. [[CrossRef](#)]
- MacDonald, D.; Crabtree, J.R.; Wiesinger, G.; Dax, T.; Stamou, N.; Fleury, P.; Gutierrez Lazpita, J.; Gibon, A. Agricultural abandonment in mountain areas of Europe: Environmental consequences and policy response. *J. Environ. Manag.* **2000**, *59*, 47–69. [[CrossRef](#)]
- Zhang, Y.; Min, Q.; Zhang, C.; He, L.; Zhang, S.; Yang, L.; Tian, M.; Xiong, Y. Traditional culture as an important power for maintaining agricultural landscapes in cultural heritage sites: A case study of the Hani terraces. *J. Cult. Herit.* **2017**, *25*, 170–179. [[CrossRef](#)]
- Yan, J.; Yang, Z.; Li, Z.; Li, X.; Xin, L.; Sun, L. Drivers of cropland abandonment in mountainous areas: A household decision model on farming scale in Southwest China. *Land Use Policy* **2016**, *57*, 459–469. [[CrossRef](#)]
- Shi, T.; Li, X.; Xin, L.; Xu, X. The spatial distribution of farmland abandonment and its influential factors at the township level: A case study in the mountainous area of China. *Land Use Policy* **2018**, *70*, 510–520. [[CrossRef](#)]
- Prishchepov, A.V.; Müller, D.; Dubinin, M.; Baumann, M.; Radeloff, V.C. Determinants of agricultural land abandonment in post-Soviet European Russia. *Land Use Policy* **2013**, *30*, 873–884. [[CrossRef](#)]
- Meyfroidt, P. Approaches and terminology for causal analysis in land systems science. *J. Land Use Sci.* **2016**, *11*, 501–522. [[CrossRef](#)]
- Zaragozí, B.; Rabasa, A.; Rodríguez-Sala, J.J.; Navarro, J.T.; Belda, A.; Ramón, A. Modelling farmland abandonment: A study combining GIS and data mining techniques. *Agric. Ecosyst. Environ.* **2012**, *155*, 124–132. [[CrossRef](#)]

27. Estel, S.; Kuemmerle, T.; Alcántara, C.; Levers, C.; Prishchepov, A.; Hostert, P. Mapping farmland abandonment and recultivation across Europe using MODIS NDVI time series. *Remote Sens. Environ.* **2015**, *163*, 312–325. [[CrossRef](#)]
28. Alcántara, C.; Kuemmerle, T.; Baumann, M.; Bragina, E.V.; Griffiths, P.; Hostert, P.; Knorn, J.; Müller, D.; Prishchepov, A.V.; Schierhorn, F.; et al. Mapping the extent of abandoned farmland in Central and Eastern Europe using MODIS time series satellite data. *Environ. Res. Lett.* **2013**, *8*, 035035. [[CrossRef](#)]
29. De Fries, R.S.; Hansen, M.; Townshend, J.R.G.; Sohlberg, R. Global land cover classifications at 8 km spatial resolution: The use of training data derived from Landsat imagery in decision tree classifiers. *Int. J. Remote Sens.* **1998**, *19*, 3141–3168. [[CrossRef](#)]
30. Dara, A.; Baumann, M.; Kuemmerle, T.; Pflugmacher, D.; Rabe, A.; Griffiths, P.; Hölzel, N.; Kamp, J.; Freitag, M.; Hostert, P. Mapping the timing of cropland abandonment and recultivation in northern Kazakhstan using annual Landsat time series. *Remote Sens. Environ.* **2018**, *213*, 49–60. [[CrossRef](#)]
31. Yin, H.; Prishchepov, A.V.; Kuemmerle, T.; Bleyhl, B.; Buchner, J.; Radeloff, V.C. Mapping agricultural land abandonment from spatial and temporal segmentation of Landsat time series. *Remote Sens. Environ.* **2018**, *210*, 12–24. [[CrossRef](#)]
32. Prishchepov, A.V.; Radeloff, V.C.; Dubinin, M.; Alcántara, C. The effect of Landsat ETM/ETM+ image acquisition dates on the detection of agricultural land abandonment in Eastern Europe. *Remote Sens. Environ.* **2012**, *126*, 195–209. [[CrossRef](#)]
33. Immitzer, M.; Vuolo, F.; Atzberger, C. First Experience with Sentinel-2 Data for Crop and Tree Species Classifications in Central Europe. *Remote Sens.* **2016**, *8*, 166. [[CrossRef](#)]
34. Gorelick, N.; Hancher, M.; Dixon, M.; Ilyushchenko, S.; Thau, D.; Moore, R. Google Earth Engine: Planetary-scale geospatial analysis for everyone. *Remote Sens. Environ.* **2017**, *202*, 18–27. [[CrossRef](#)]
35. dos Santos, E.P.; da Silva, D.D.; do Amaral, C.H.; Fernandes-Filho, E.I.; Dias, R.L.S. A Machine Learning approach to reconstruct cloudy affected vegetation indices imagery via data fusion from Sentinel-1 and Landsat 8. *Comput. Electron. Agric.* **2022**, *194*, 106753. [[CrossRef](#)]
36. Zhang, X.; Wu, B.; Ponce-Campos, G.E.; Zhang, M.; Chang, S.; Tian, F. Mapping up-to-Date Paddy Rice Extent at 10 M Resolution in China through the Integration of Optical and Synthetic Aperture Radar Images. *Remote Sens.* **2018**, *10*, 1200. [[CrossRef](#)]
37. Zanaga, D.; Van De Kerchove, R.; De Keersmaecker, W.; Souverijns, N.; Brockmann, C.; Quast, R.; Wevers, J.; Grosu, A.; Paccini, A.; Vergnaud, S.; et al. ESA WorldCover 10 m 2020 v100. Available online: <https://data.apps.fao.org/catalog/dataset/378e9df5-3814-4a80-bb47-e25df0543634> (accessed on 25 April 2024).
38. Karra, K.; Kontgis, C.; Statman-Weil, Z.; Mazzariello, J.C.; Mathis, M.; Brumby, S.P. Global land use/land cover with Sentinel 2 and deep learning. In Proceedings of the 2021 IEEE International Geoscience and Remote Sensing Symposium IGARSS, Brussels, Belgium, 11–16 July 2021; pp. 4704–4707.
39. Zhang, X.; Liu, L.; Chen, X.; Gao, Y.; Xie, S.; Mi, J. GLC\_FCS30: Global land-cover product with fine classification system at 30&thinspm using time-series Landsat imagery. *Earth Syst. Sci. Data* **2021**, *13*, 2753–2776. [[CrossRef](#)]
40. Yang, J.; Huang, X. The 30&thinspm annual land cover dataset and its dynamics in China from 1990 to 2019. *Earth Syst. Sci. Data* **2021**, *13*, 3907–3925. [[CrossRef](#)]
41. Rouse, J.W.; Haas, R.H.; Schell, J.A.; Deering, D.W. Monitoring vegetation systems in the great plains with ERTS. *NASA Spec. Publ.* **1973**, *351*, 309.
42. Olsen, V.M.; Fensholt, R.; Olofsson, P.; Bonifacio, R.; Butsic, V.; Druce, D.; Ray, D.; Prishchepov, A.V. The impact of conflict-driven cropland abandonment on food insecurity in South Sudan revealed using satellite remote sensing. *Nat. Food* **2021**, *2*, 990–996. [[CrossRef](#)]
43. Eklund, L.; Degerald, M.; Brandt, M.; Prishchepov, A.; Pilesjö, P. How conflict affects land use: Agricultural activity in areas seized by the Islamic State. *Environ. Res. Lett.* **2017**, *12*, 054004. [[CrossRef](#)]
44. Inglada, J.; Vincent, A.; Arias, M.; Marais-Sicre, C. Improved Early Crop Type Identification By Joint Use of High Temporal Resolution SAR And Optical Image Time Series. *Remote Sens.* **2016**, *8*, 362. [[CrossRef](#)]
45. Van Tricht, K.; Gobin, A.; Gilliams, S.; Piccard, I. Synergistic use of radar Sentinel-1 and optical Sentinel-2 imagery for crop mapping: A case study for Belgium. *Remote Sens.* **2018**, *10*, 1642. [[CrossRef](#)]
46. dos Santos, E.P.; Da Silva, D.D.; do Amaral, C.H. Vegetation cover monitoring in tropical regions using SAR-C dual-polarization index: Seasonal and spatial influences. *Int. J. Remote Sens.* **2021**, *42*, 7581–7609. [[CrossRef](#)]
47. Frison, P.-L.; Fruneau, B.; Kmiha, S.; Soudani, K.; Dufrene, E.; Le Toan, T.; Koleck, T.; Villard, L.; Mougou, E.; Rudant, J.-P. Potential of Sentinel-1 Data for Monitoring Temperate Mixed Forest Phenology. *Remote Sens.* **2018**, *10*, 2049. [[CrossRef](#)]
48. Hird, J.N.; DeLancey, E.R.; McDermid, G.J.; Kariyeva, J. Google Earth Engine, Open-Access Satellite Data, and Machine Learning in Support of Large-Area Probabilistic Wetland Mapping. *Remote Sens.* **2017**, *9*, 1315. [[CrossRef](#)]
49. Nasirzadehdizaji, R.; Balik Sanli, F.; Abdikan, S.; Cakir, Z.; Sekertekin, A.; Ustuner, M. Sensitivity Analysis of Multi-Temporal Sentinel-1 SAR Parameters to Crop Height and Canopy Coverage. *Appl. Sci.* **2019**, *9*, 655. [[CrossRef](#)]
50. Zhou, J.; Jia, L.; Menenti, M. Reconstruction of global MODIS NDVI time series: Performance of Harmonic ANalysis of Time Series (HANTS). *Remote Sens. Environ.* **2015**, *163*, 217–228. [[CrossRef](#)]
51. Jordan, C.F. Derivation of Leaf-Area Index from Quality of Light on the Forest Floor. *Ecology* **1969**, *50*, 663–666. [[CrossRef](#)]
52. Rikimaru, A.; Roy, P.S.; Miyatake, S. Tropical forest cover density mapping. *Trop. Ecol.* **2002**, *43*, 39–47.
53. Kolluru, V.; John, R.; Saraf, S.; Chen, J.; Hankerson, B.; Robinson, S.; Kussainova, M.; Jain, K. Gridded livestock density database and spatial trends for Kazakhstan. *Sci. Data* **2023**, *10*, 839. [[CrossRef](#)] [[PubMed](#)]

54. Cramer, V.A.; Hobbs, R.J.; Standish, R.J. What's new about old fields? Land abandonment and ecosystem assembly. *Trends Ecol. Evol.* **2008**, *23*, 104–112. [[CrossRef](#)] [[PubMed](#)]
55. Prishchepov, A.V.; Schierhorn, F.; Löw, F. Unraveling the Diversity of Trajectories and Drivers of Global Agricultural Land Abandonment. *Land* **2021**, *10*, 97. [[CrossRef](#)]
56. Wang, J.-F.; Zhang, T.-L.; Fu, B.-J. A measure of spatial stratified heterogeneity. *Ecol. Indic.* **2016**, *67*, 250–256. [[CrossRef](#)]
57. Song, Y.; Wang, J.; Ge, Y.; Xu, C. An optimal parameters-based geographical detector model enhances geographic characteristics of explanatory variables for spatial heterogeneity analysis: Cases with different types of spatial data. *GIScience Remote Sens.* **2020**, *57*, 593–610. [[CrossRef](#)]
58. Venkatesh, K.; John, R.; Chen, J.; Xiao, J.; Amirkhiz, R.G.; Giannico, V.; Kussainova, M. Optimal ranges of social-environmental drivers and their impacts on vegetation dynamics in Kazakhstan. *Sci. Total Environ.* **2022**, *847*, 157562. [[CrossRef](#)] [[PubMed](#)]
59. Li, H.; Song, W. Cropland Abandonment and Influencing Factors in Chongqing, China. *Land* **2021**, *10*, 1206. [[CrossRef](#)]
60. Alcantara, C.; Kuemmerle, T.; Prishchepov, A.V.; Radeloff, V.C. Mapping abandoned agriculture with multi-temporal MODIS satellite data. *Remote Sens. Environ.* **2012**, *124*, 334–347. [[CrossRef](#)]
61. Queiroz, C.; Beilin, R.; Folke, C.; Lindborg, R. Farmland abandonment: Threat or opportunity for biodiversity conservation? A global review. *Front. Ecol. Environ.* **2014**, *12*, 288–296. [[CrossRef](#)] [[PubMed](#)]
62. Qiu, B.; Yang, X.; Tang, Z.; Chen, C.; Li, H.; Berry, J. Urban expansion or poor productivity: Explaining regional differences in cropland abandonment in China during the early 21st century. *Land Degrad. Dev.* **2020**, *31*, 2540–2551. [[CrossRef](#)]
63. Bai, M.; Zhou, S.; Tang, T. A Reconstruction of Irrigated Cropland Extent in China from 2000 to 2019 Using the Synergy of Statistics and Satellite-Based Datasets. *Land* **2022**, *11*, 1686. [[CrossRef](#)]
64. Ding, S.; Li, M.; Wang, X.; Li, L.; Wu, R.; Huang, H. The Use of Time Series Remote Sensing Data to Analyze the Characteristics of Non-agriculture Farmland and Their Driving Factors in Fuzhou. *Remote Sens. Technol. Appl.* **2022**, *37*, 550–563. [[CrossRef](#)]
65. Jiang, C.; Song, W. Degree of Abandoned Cropland and Socioeconomic Impact Factors in China: Multi-Level Analysis Model Based on the Farmer and District/County Levels. *Land* **2022**, *11*, 8. [[CrossRef](#)]
66. Wang, X.; Zhao, D. Study on the Causes of Differences in Cropland Abandonment Levels among Farming Households Based on Hierarchical Linear Model—13,120 Farming Households in 26 Provinces of China as an Example. *Land* **2023**, *12*, 1791. [[CrossRef](#)]
67. Jin, X.; Xiang, X.; Guan, X.; Wu, X.; Bai, Q.; Zhou, Y. Assessing the relationship between the spatial distribution of land consolidation projects and farmland resources in China, 2006–2012. *Food Secur.* **2017**, *9*, 889–905. [[CrossRef](#)]
68. Hong, C.; Jin, X.; Fan, Y.; Xiang, X.; Cao, S.; Chen, C.; Zheng, G.; Zhou, Y. Determining the effect of land consolidation on agricultural production using a novel assessment framework. *Land Degrad. Dev.* **2020**, *31*, 356–371. [[CrossRef](#)]
69. Guo, A.; Yue, W.; Yang, J.; Xue, B.; Xiao, W.; Li, M.; He, T.; Zhang, M.; Jin, X.; Zhou, Q. Cropland abandonment in China: Patterns, drivers, and implications for food security. *J. Clean. Prod.* **2023**, *418*, 138154. [[CrossRef](#)]

**Disclaimer/Publisher's Note:** The statements, opinions and data contained in all publications are solely those of the individual author(s) and contributor(s) and not of MDPI and/or the editor(s). MDPI and/or the editor(s) disclaim responsibility for any injury to people or property resulting from any ideas, methods, instructions or products referred to in the content.